Thermodynamic investigation of quasi-isothermal air compression/expansion for energy storage

Ghady Dib, Philippe Haberschill, Romuald Rullière, Rémi Revellin

Thermodynamic investigation of quasi-isothermal air compression/expansion for energy storage

Ghady DIB[1], Philippe HABERSCHILL[1], Romuald RULLIERE[1], Rémi REVELLIN[1*]

[1]Univ Lyon, INSA Lyon, CNRS, CETHIL, UMR5008, 69621 Villeurbanne, France
[*](remi.revellin@insa-lyon.fr)

ABSTRACT

Compressed air energy storage system is a promising solution in the energy storage field: it is characterized by a high reliability, low environmental impact and a remarkable energy density. This study focuses on two of the advanced technologies in the isothermal compressed air energy storage systems developed by LightSail Energy (mechanical piston with water injection) and Enairys Powertech (liquid piston with integrated heat exchanger). A first numerical model based on thermodynamic and energy analysis of the concerned technologies is presented in this work. These mathematical models enabled the comprehension of the main operation of these technologies and therefore having many orders of magnitudes of different physical parameters such as air/water temperature, air pressure, compensated/recovered work, heat absorbed/released, droplet diameter and heat transfer coefficient. Mechanical piston with water injection technology showed to be favorable to the production of hot water (15 °C water gradient) during air compression and cold water during air expansion, where liquid piston with integrated heat exchanger represented a strong isothermal compression and expansion with a minimal air/water temperature gradient (1 °C / 0.2 °C).

Nomenclature

a	length constant
c	specific heat capacity, $J.kg^{-1}.K^{-1}$
D	diameter, m
h	specific enthalpy, $J.kg^{-1}$
he	heat transfer coefficient, $W.m^{-2}.K^{-1}$
K	thermal conductivity, $W.m^{-1}.K^{-1}$
L	length, m
$\dot{m}$	mass flow rate, $kg.s^{-1}$
n	polytropic index
nu	number of water droplets
nt	number of tubes
P	pressure, Pa
Q	heat transfer, J
$\dot{Q}$	heat transfer rate, W
ra	radius, m
S	surface, m^2
t	time, s
T	temperature, K
U	internal energy, J
V	volume, m^3
v	specific volume, $m^3.kg^{-1}$
W	work, J

Greek letters

Δ	delta
ρ	density, $kg.m^{-3}$
η	efficiency
$\dot{W}$	mechanical power, $J.s^{-1}$
x	absolute humidity

Subscripts

av	average
c	compressor
cy	cycle
Dr	droplets
DA	dry air
HA	humid air
in	input
out	output
p	constant pressure
pol	polytropic
SAT	saturated
t	turbine
tot	total
tu	tube
va	vapor
v	constant volume

Superscript

w	water
wv	water vapor

Abbreviation

AA-CAES	advanced adiabatic compressed air energy
CAES	compressed air energy storage
C-CAES	classical compressed air energy storage
DD	droplet diameter
TC	heat transfer coefficient
I-CAES	isothermal compressed air energy storage
ML	mass loading
NTU	number of transfer units
TD	tube diameter
VR	volume ratio

1. Introduction

1.1 Energy context overview

Renewable energy development is a major challenge in today's context with energy demand growth, potential depletion of fossil resources and the urgency of reducing greenhouse gas emissions. The European Union has decided to achieve a share of renewable energies in its gross final energy consumption of at least 32 % by 2030 [1]. Based on the RTE electricity report [2], the renewable coverage of power demand rose from 18.5% in 2017 to 22.7 % in 2018 as seen in Figure 1. This high record is a direct consequence of government policies that motivated to increase the installed capacity of based on renewable energy. This coverage of 22.7 % can be divided into four different segments: 58.1 % for hydropower, 25.6 % for wind power, 9.4 % for solar power and 6.9% for bioenergy [2].

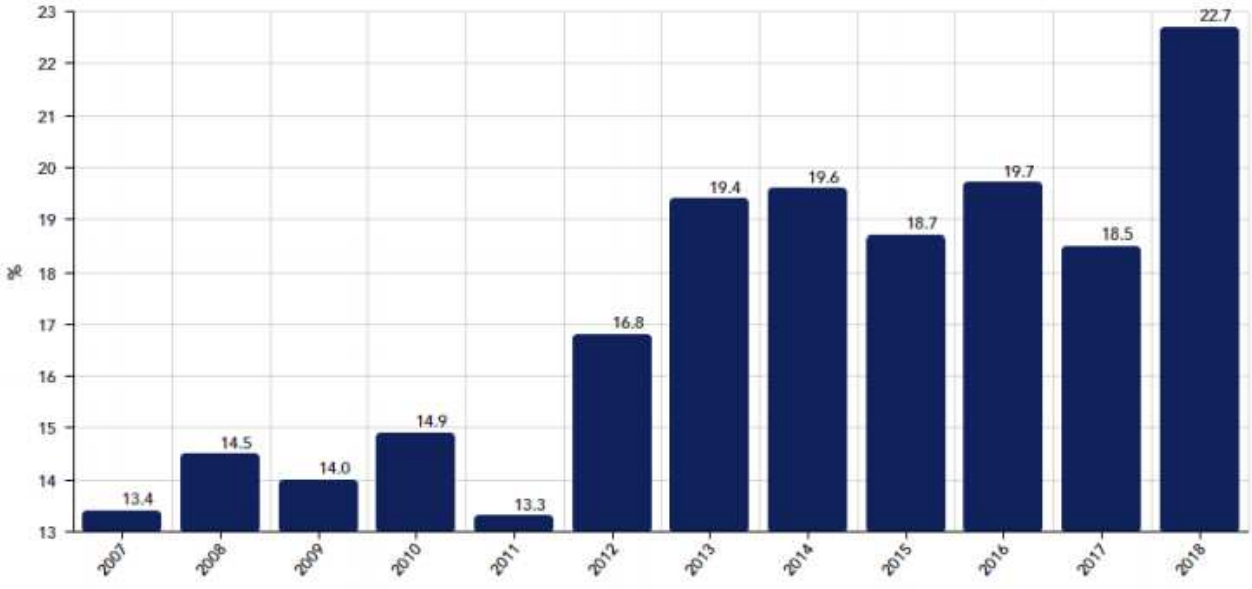

Figure 1: The share of annual electricity production from renewable energy sources as a percentage of total demand [2]

Renewable resources intermittency represents a major obstacle and challenge to their extensive penetration into the grid. The energy storage technology can be a solution for stabilizing the fluctuating energy production to meet the energy demand [3], [4]. This energy balance is achieved by allowing excess energy production to be saved for periods of higher customer demand. These days high electricity demand is answered through the import of electricity, the use of gas/fuel power and pumped-storage hydroelectricity (PSH) plants. The deployment of other energy storage systems would lower several environmental side effects such

as blocking, diverting or changing the natural course of river systems and therefore an important migration route for fish. The compressed air energy storage system (CAES) is one of the most promising technologies of the field of smart grid and poly-generation in the near future [4]–[8]. CAES presents several significant advantages due to its reliability, economic feasibility and low environmental impact [4]. Energy storage technologies have been the subject of research published by "French Alternative Energies and Atomic Energy Commission" (CEA) where CAES is presented as the technology with the lowest investment cost per power and energy unit (€/kW, €/kWh) compared to Li-ion batteries and PSH energy storage technology [9].

1.2 Compressed air energy storage technology

Two power plants with compressed air storage systems are currently operating in the world: Huntorf plant in Germany built in 1978 with a capacity of 290 MW, and the McIntosh plant in the United States with a capacity of 110 MW [10]. These plants (classical CAES system) compress the air adiabatically and store it in former salt cavities or coal mines. Before compressed air expansion, an external heat source is used to raise the air temperature before entering the turbine [11]. In the case of heat management, the CAES system is called advanced adiabatic (AA-CAES) where electrical efficiency (output/input) can range from 40 to 70% depending on the heat management method resulting from air compression. In this case, the heat resulting from compression is stored to be reused during compressed air expansion, and cold resulting from expansion is stored to be reuse during next air compression cycle [12].

Geological factors control (underground storage) are limiting the development of the large-scale (> 50 MW) CAES systems. This fact motivated many researchers and private companies into the micro-CAES systems development (< 1 MW) where small high pressure and transportable air reservoir are realized. The micro quasi-isothermal CAES (I-CAES) system answers the problem of the heat releasing during the air compression and the cold during the air expansion in order to make the storage or the use of compressed air more efficient. In fact, it allows to reduce the compensated work during the air compression and to increase the work recovered during the air expansion. This system requires a continuous release of heat during the air compression and heat introduction during air expansion.

Two important innovative technologies related to micro I-CAES system were developed in order to compress/expand air with a quasi-isothermal transformation and to produce heat and cold energy: mechanical piston with water injection developed by LighSail Energy [13] and liquid

piston with integrated heat exchanger developed by Enairys Powertech [14]. In addition, SustainX developed an innovative concept where they used foam injection in order to have a quasi-isothermal air compression and expansion [15].

This article focuses on the development of the first numerical model that simulate the micro I-CAES system developed by LightSail Energy and Enairys Powertech based on the limited open access database, in order to have a better understanding of the main sizing parameters for the concerned technologies.

2. Isothermal compressed air energy storage (I-CAES) technology

I-CAES system deals with quasi-isothermal compressor/expander that are desired for high efficiency performance. Many theoretical concepts were proposed in order to improve multiple factors that have a big impact on the overall compressor/expander operation [16]–[18]. High heat transfer was a must in order to achieve nearly isothermal air compression/expansion and to circumvent the reduction in global efficiency. Water spray injection and liquid piston compression/expansion concepts were proposed, developed and completed by many researchers seeking to have the effective solution that can provide a high total surface area for heat transfer [16]–[18]. Herein, these published scientific works that are mostly similar to LightSail Energy and Enairys Powertech technologies development were used in this article as a complementary understanding of the concerned micro I-CAES system.

2.1 Overview of the micro I-CAES system developed by LightSail Energy (LSE)

In 2009, The company LightSail Energy (LSE) developed a new compressor/expander technology where quasi-isothermal air compression/expansion were introduced. Recently LSE focused on CAES aboveground storage by developing specialized high pressure carbon fiber tanks. LSE filed more than 50 patents and more than 1000 claims granted related to engine development, thermodynamics, electronics, pressure vessels and composite materials.

LSE has developed an advanced method of capturing the heat produced during the air compression and regenerating useful energy from it which will help to increase the round-trip efficiency of the energy storage system. Water is injected into the compression chamber during the compression process. The cold water absorbs the heat of compression and returns it during expansion process as illustrated in Figure 2. The regenerative air energy storage (RAES) proposed by LSE presents the following principle (Figure 2) [13]:

- Electricity drives a motor.
- The motor drives the quasi-isothermal air compressor.
- Water spray absorbs the heat released during air compression.

Energy is stored in the form of compressed air and warm water. The same mechanism operates in reverse to deliver power.

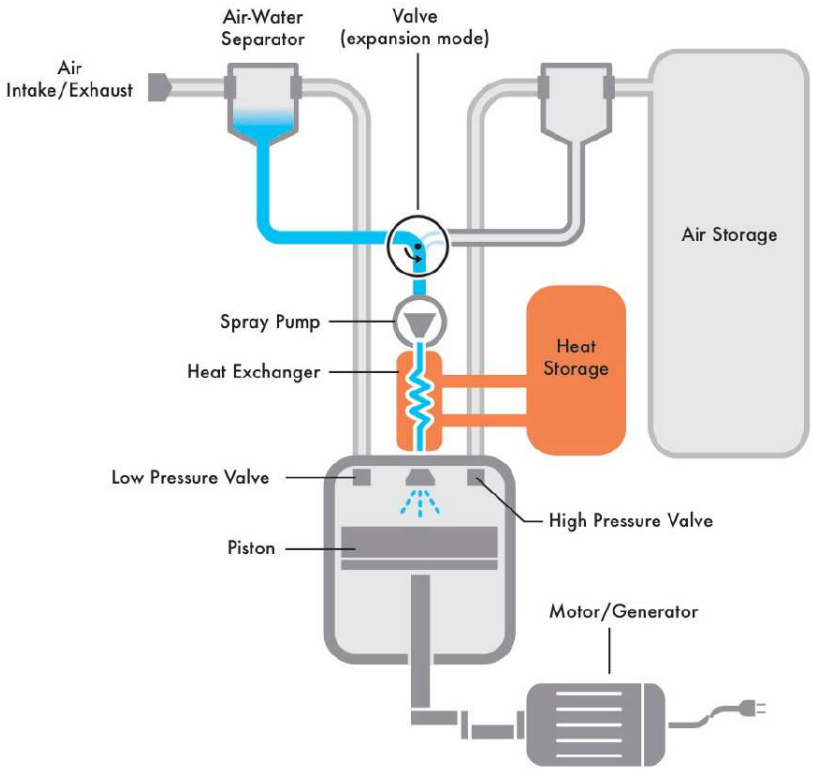

Figure 2: The RAES system operation presented by LSE

2.2 Overview of the micro I-CAES system developed by Enairys Powertech

Enairys Powertech is a Swiss startup incorporated in 2008 that develops compressed air storage solutions and energy management based on patented liquid piston compressor/expander technology. Four patents related to storage system based on liquid piston and scroll compressor/expander technology have been filed [19]. Enairys Powertech first non-commercial prototype was developed during 2011 for a 10 kW of input electricity. During the same year, they launched a pilot project with Mont-Soleil photovoltaic power plant organization and F.M.B Energie in order to develop a first commercial hydropneumatic energy storage system (HyPES) prototype of 25 kW [20]. HyPES solution concept is based on combining the new liquid piston

compression/expansion concept with a specific power electronics and control units as seen in Figure 3.

Figure 3: Enairys storage solution technology (Left) and energy conversion chamber (Right) [21]

Three modules can be defined in the global system (Figure 3 and Figure 4):

- Conversion and management module (center): it manages and transforms electrical energy to compressed air. It integrates the motor/generator, the various conversion stages (reversible pumps and liquid piston chambers) as well as the control unit. The size of this module depends on the maximum power (kW) of the system.
- Storage module (left): High pressure cylinders in steel or carbon fiber are used to store the compressed air. The total volume defines the energy capacity of the system (kWh).
- Water storage module (Right): The water unit has the role of cleaning and maintaining the system water at room temperature. It basically consists of a tank, a filter and a heat exchanger with the ambient air.

Based on the thesis work of Lemofouet [14], water is used as a "liquid piston" to compress the air along with cooling it and to expand the air by heating it simultaneously. An exchanger (tubes) is placed in the compression/expansion chamber to ensure an exchange surface between air and water. An electric motor and a reversible pump are connected to the chamber in order to let the water circulate in the tubes. In expansion mode, the motor is used as a generator to recover the mechanical energy from the pump (used as expander) and convert it into electricity [22].

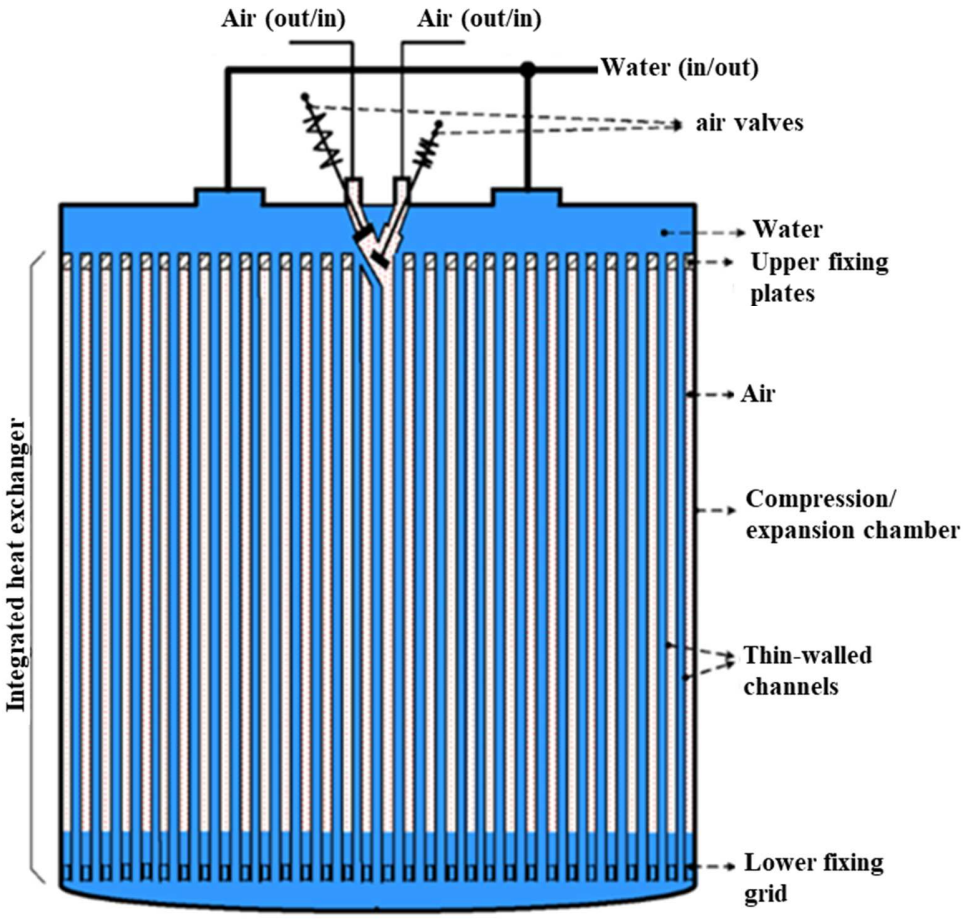

Figure 4: Energy conversion chamber developed by Enairys Powertech [21]

From Figure 5 to Figure 8 the air liquid piston compression process is described and is divided into four phases:

1. Humid air is introduced into the compression chamber. At the same time, water in the tubes is evacuated using a reversible pump. Air water interface moves down the chamber during this process (Figure 5).
2. Cold water is injected into the tubes. Air water interface moves upward of the chamber. The air in the chamber between the tubes is compressed (Figure 6).
3. When the pressure in the chamber reaches the discharge pressure, the air is evacuated through the air outlet valve. Water is injected to ensure the delivery of compressed air, especially when the pressure difference (chamber-reservoir) is low (Figure 7).
4. At the end of compressed air discharge, air input and water output valves are opened. This fact creates pressure drop in the chamber (Figure 8).

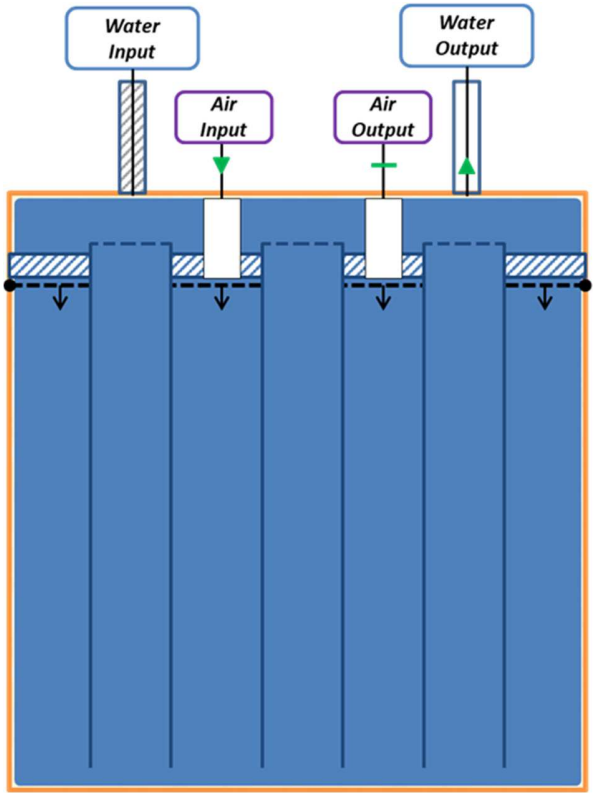

Figure 5: Phase 1 of the compression cycle

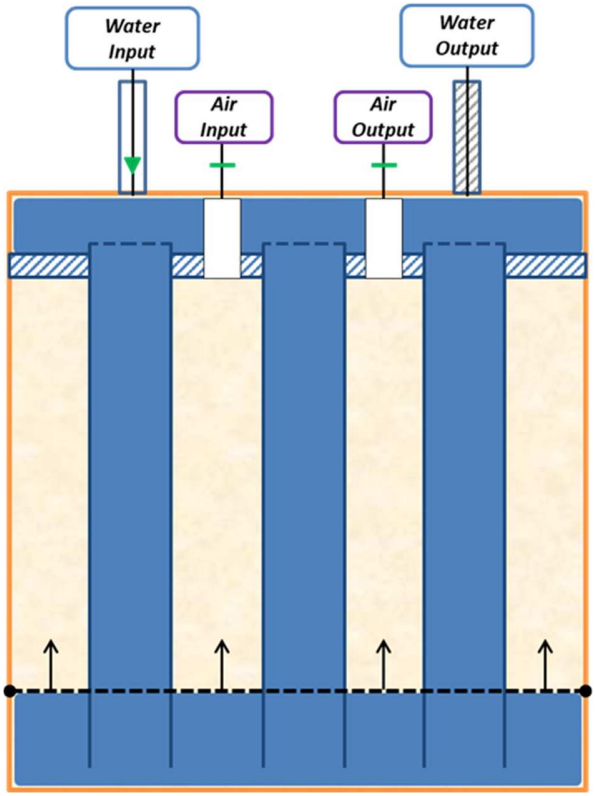

Figure 6: Phase 2 of the compression cycle

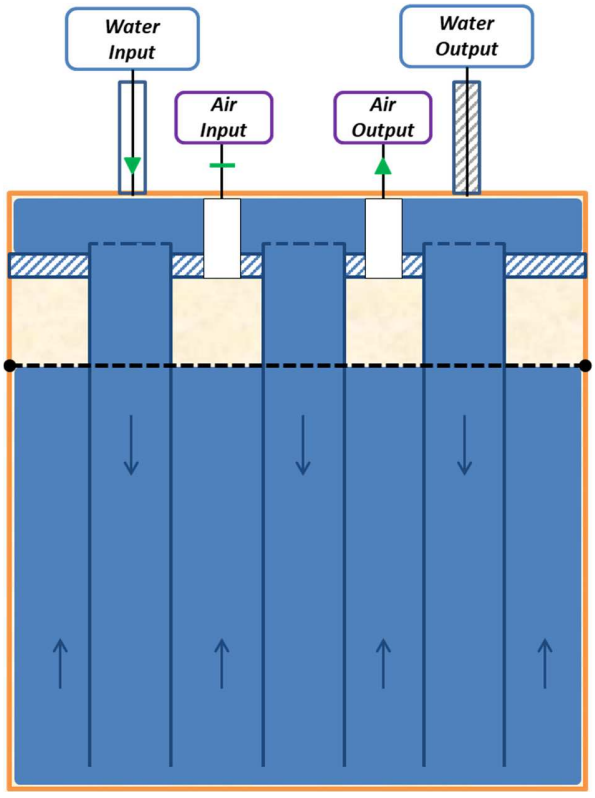

Figure 7: Phase 3 of the compression cycle

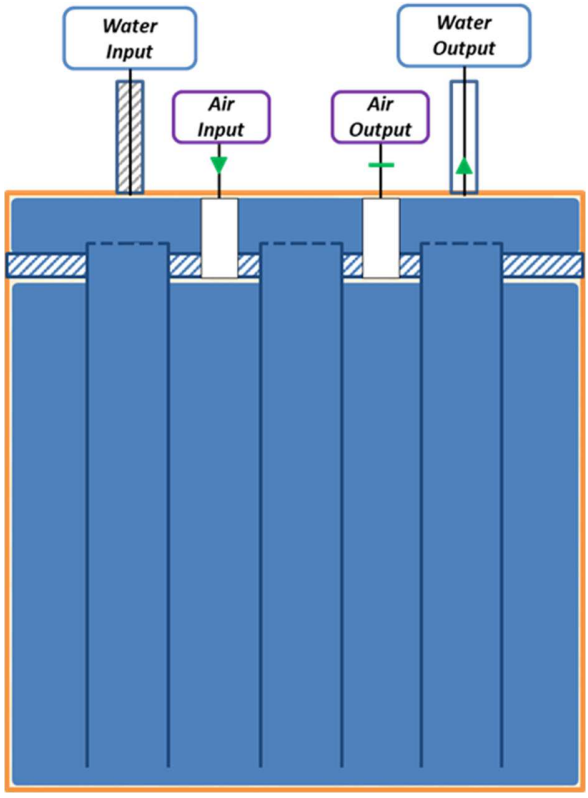

Figure 8: Phase 4 of the compression cycle

3. Theoretical investigation

3.1 Numerical analysis of the mechanical piston compressor/expander with water injection

The quasi-isothermal compressor/expander simulated in this work is based on solving the principles of energy and mass conservation applied to the flows passing through the compressor/expander in a steady state: humid air at input temperature (T_{in}) and water in the form of droplets at input temperature (T_{in}^{w}) (Figure 9). Air is considered for all the parameters calculated in this chapter (temperature, pressure, mass, mass flow rate…) while the superscript "w" is written to indicate water as the working fluid.

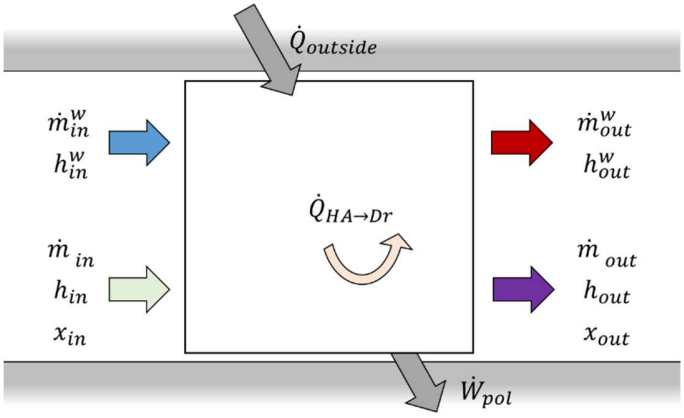

Figure 9: Conservation of energy for a steady-flow, open system

3.1.1 Mechanical piston compressor/expander numerical model assumptions

The following assumptions have been taken into account:

- Perfect gas is considered.
- Heat transfers between the compression/expansion chamber and the outside are taken into account using a single uniform wall temperature T_{wall}.
- Air compression phase is cooled by heating cold water droplets.
- Air expansion phase is heated by cooling hot water droplets.
- The compressor outlet air wet temperature is equal to that of the water.
- Mass exchange between air and injected water droplets during compression/expansion will be guided by the difference in water vapor pressure contained in the air and in the vicinity of the water droplets (see Appendix).
- Water is introduced into the compressor along with air in the form of incompressible droplets which heat up and vaporize or condensate without disappearing.

- The kinetic energy of the air is neglected.

Figure 10 shows the PV diagram for the air compression and expansion cycles.

- Air suction (1→2) and compressed air introduction (1'→2') phases are considered to be isothermal and isobaric processes.
- Compressed air discharge (3→4) and expanded air discharge (4'→5') phases are considered to be also isothermal and isobaric processes.
- An isochoric expansion (3'→4') is considered after the compressed air expansion phase (2'→3').

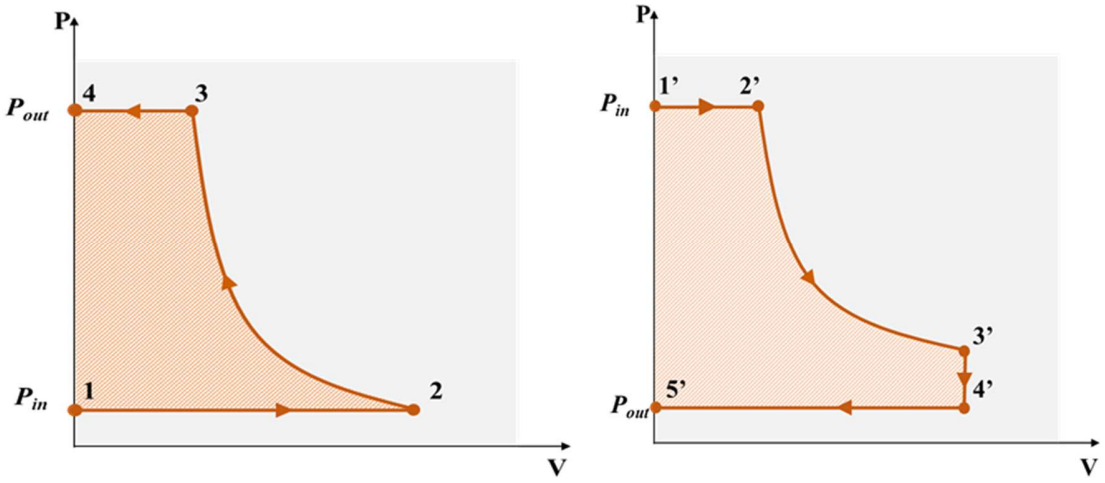

Figure 10: PV diagram of the air compression (left) and expansion (right) cycles

3.1.2 Analytical model of the mechanical piston compressor with water injection

- **Air energy conservation**

The energy conservation for humid air running through the compressor (the heat transfer rates are written as absolute value):

$$\dot{m}_{DA}(h_{out} - h_{in}) = \dot{m}_{DA}\frac{1}{\eta_{pol}}\frac{n_c}{n_c - 1}(P_{out}v_{out} - P_{in}v_{in}) - \dot{Q}_{HA\to Dr} + he_{wa}\,S_{wa}(T_{wa} - T_{av}) + \dot{m}_{DA}\,(x_{out} - x_{in})\,h_{va} \quad (1)$$

Where $\dot{Q}_{HA\leftrightarrow Dr}$ is the thermal energy shared between the humid air and water droplets inside the mechanical cylinder chamber during the air compression phase. $\dot{m}_{DA}$ is the dry air mass flow rate entering and leaving the chamber at the respective enthalpies h_{in} and h_{out} and at respective absolute humidity x_{in} and x_{out}. Internal wall conductance is represented by $he_{wa}\,S_{wa}$ with

internal wall temperature T_{wa} (this term is negligible if wall is considered as adiabatic). The average humid air temperature T_{av} is given by the following equation:

$$T_{av} = \frac{T_{out} + T_{in}}{2} \tag{2}$$

The humid air enthalpy per unit dry air mass is described as follow:

$$h_{HA} = c_p T + h_{va} x \tag{3}$$

Where the specific enthalpy for the steam (or vapor) is shown in the equation below:

$$h_{va} = \Delta h_{lv} + c_{p,va} T \tag{4}$$

Δh_{lv} is the specific enthalpy of water vaporization at 0°C. The two enthalpy equations described above are used for air input and output of the compressor. Absolute humidity x of the humid air is a function of the temperature and of the air relative humidity at the compressor inlet. Considering the wet air temperature equal to that of water, the compressor outlet absolute humidity is obtained from the following:

$$x_{out} = d \frac{P_{SAT}^{wv}}{P_{out} - P_{SAT}^{wv}} \tag{5}$$

With *d* (equal to 0.62198) is the water vapor relative density (to the air). It should be mentioned that the "*SAT*" nomenclature does not refer to all the air particles founded in the cylinder chamber. In fact, it refers to the air particles located around the water droplet at the outlet of the compressor/expander. Therefore, the saturated water vapor pressure P_{SAT}^{wv} at outlet water temperature T_{out}^{w} is given by the following equation:

$$\ln(P_{SAT}^{wv}) = \frac{a_0}{T_{out}^{w}} + a_1 + a_2 T_{out}^{w} + a_3 (T_{out}^{w})^2 + a_4 ln(T_{out}^{w}) \tag{6}$$

The a_i values are given in Table 1.

Table 1: Coefficients values for the calculation of the saturation vapor pressure of water [23]

a_0 (K)	a_1	a_2(K^{-1})	a_3(K^{-2})	a_4
-6096.9385	21.2409642	-2.711 193x10^{-2}	1.673952x10^{-2}	2.433502

- **Air mass conservation**

The dry air mass flow rate sucked by the compressor is deduced from the effective volumetric flow rate ($\dot{V}_c$) generated by:

$$\dot{m}_{DA} = \frac{\dot{V}_c}{v_{in}} \tag{7}$$

With v_{in} the volume of wet air per unit dry air mass.

- **Water energy conservation**

$$\dot{m}^w_{out}\, h^w_{out} - \dot{m}^w_{in}\, h^w_{in} = \dot{Q}_{HA\leftrightarrow Dr} - \dot{m}_{DA}\,(x_{out} - x_{in})\,(h_{va}) \tag{8}$$

where $\dot{m}^w_{out}$ and $\dot{m}^w_{in}$ the outlet and inlet mass flow rates of the water droplets with respective specific enthalpies h^w_{out} and h^w_{in}.

- **Water mass conservation**

$$\dot{m}^w_{in} = \rho^w\, \dot{nu}_{Dr}\, \frac{4}{3}\pi\,(ra_{Dr})^3_{in} = \dot{m}_{DA}\,(x_{out} - x_{in}) + \dot{m}^w_{out} \tag{9}$$

where $\dot{nu}_{Dr}$ is the number of water droplets per second, ρ^w is the water density and ra_{Dr} is the droplet radius.

$$\dot{m}^w_{out} = \rho^w\, \dot{nu}_{Dr}\, \frac{4}{3}\pi\ \ (ra_{Dr})^3_{out} \tag{10}$$

- **Complementary equations**

The heat transfer exchanged between water and humid air is given by the following equation:

$$\dot{Q}_{HA\rightarrow Dr} = he\ 4\,\pi (ra_{Dr})^2_{av}\, nu_{Dr}(T_{av} - T^w_{av}) \tag{11}$$

where T_{av}, T^w_{av} are the humid air and water average temperatures and $(ra_{Dr})_{av}$ is the droplet average radius. The heat transfer coefficient was studied numerically and measured experimentally by many researchers. Most of the water spray injection numerical models used the Ranz-Marshall correlation which indicated convective heat transfer for spheres as Qin and Loth [18] and Odukomaiya [24] did in their works. The range of heat transfer coefficient applied in this study is however based on an experimental work conducted by Guanwei [16] where a transient temperature measurement method was developed to investigate the heat transfer behavior while cooling the air by injecting water spray. Based on the measurements carried out

by Guanwei [16], the value of the heat transfer coefficient is in the range of 10 $W.m^{-2}.K^{-1}$ - 250 $W.m^{-2}.K^{-1}$. Furthermore the water droplet number is expressed as follows:

$$nu_{Dr} = \dot{n}u_{Dr}\, t_{ST} \tag{12}$$

t_{st} is the water droplets residence time in the compressor chamber during air compression phase which will depend on the rotation speed (among other parameters). It is also necessary to write the energy conservation for the compressor wall as the following (wall conduction neglected due to the assumption of low wall thermal resistance with respect to the thermal resistance between the ambient air and the outer wall of the compressor):

$$\begin{aligned} \dot{Q}_{conduction} = -he_{wa} S_{wa}\,(T_{wa} - T_{av}) + \\ he_{outside}\, S_{outside}\,(T_{\infty} - T_{wa}) = 0 \end{aligned} \tag{13}$$

Where $he_{outside}\, S_{outside}$ is the external heat transfer conductance of the compressor and T_{∞} is the external temperature. With this latter equation, the outside heat transfer rate can be expressed as follows:

$$\dot{Q}_{outside} = he_{wa} S_{wa}\,(T_{wa} - T_{av}) = KS\,(T_{\infty} - T_{av}) \tag{14}$$

With *KS* the global heat transfer conductance ($KS = [1/(he_{wa}S_{wa}) + 1/(he_{outside}\, S_{outside})]^{-1}$).

Equation (1) becomes:

$$\begin{aligned} \dot{m}_{DA}(h_{out} - h_{in}) \\ = \dot{W}_{real} - \dot{Q}_{HA\to Dr} + \dot{m}_{DA}\,(x_{out} - x_{in})\, h_{va} + \dot{Q}_{outside} \end{aligned} \tag{15}$$

With the total real power rate:

$$\dot{W}_{real} = \dot{m}_{DA} \frac{1}{\eta_p} \frac{n_c}{n_c - 1} (P_{out} v_{out} - P_{in} v_{in}) \tag{16}$$

3.1.3 Analytical model of the mechanical piston expander with water injection

The analytical model of the mechanical piston expander with water injection is similar to the compressor model detailed above. Based on the assumption regarding the isochoric expansion, multiple different equations are added in the section below in order to build the expander model. In the expander case, Eq. (1) that presents the energy conservation for humid air running through the expander, is as follows:

$$\dot{m}_{DA}(h_{out} - h_{in}) = \left[\frac{1}{n_t - 1}(\eta_{pol})(P_{in}V_{2'})[(VR)^{n_t-1} - 1] + P_{out}V_{4'} - P_{in}V_{2'}\right]{}^{1}/_{\Delta t_{cy}} - \dot{Q}_{HA\to Dr} + he_{wa}\, S_{wa}(T_{wa} - T_{av}) + \dot{m}_{DA}(x_{out} - x_{in})\, h_{va} \quad (17)$$

From above equation, VR is the volume ratio ($\frac{V_{2'}}{V_{3'}}$), Δt_{cy} is the time needed to expand the compressed air and the rest of the variables are the same used as in Eq. (1). Since the expanded air discharge phase (4'→5') is isothermal, therefore the outlet air temperature is equal to the following:

$$T_{out} = T_{4'} = T_{3'}\left(\frac{P_{out}}{P_{3'}}\right) = T_{in}VR^{(n_t-1)}\left(\frac{P_{out}}{P_{in}VR^{(n_t)}}\right) \quad (18)$$

The compressed air mass flow rate introduced into the expander, is a function of the volume ratio VR as described in the following equation:

$$\dot{m}_{DA} = VR\frac{\dot{V}_c}{v_{in}} \quad (19)$$

3.2 Numerical analysis of the liquid piston compressor and expander with integrated heat exchanger

The quasi-isothermal liquid piston compressor/expander simulated in this section is based on solving the principles of energy and mass conservation applied to the air at input temperature (T_A) and water at input temperature (T_{F+}^{w}) passing through the compressor/expander as seen in Figure 11.

3.2.1 Liquid piston compressor/expander numerical model assumptions

The following assumptions have been taken into account:

- Perfect gas is considered.
- Air compression phase is cooled by heating the water tubes inside the chamber.
- Inlet water mass flow rate introduced into the liquid piston chamber is equal to outlet water mass flow rate leaving the chamber ($\dot{m}_{in}^{w} = \dot{m}_{out}^{w} = \dot{m}^{w} = \left(\frac{V_B\, \rho_{F+}^{w}}{t_{cy}}\right)_{comp}$).
- Air volume introduced to compressor/expander is equal to water volume pumped into the compression/expansion chamber.

- Water is considered incompressible and non-expandable.
- The heat transfer at the air-water interface is negligible taking into account the length to diameter ratio of the air space (space between the tubes) which is important.
- The heat transfer coefficient is assumed to be the same during the three phases of the compression cycle (suction + compression + discharge).
- The dead volume is considered to be equal to zero at the end of compressed air discharge phase (State E').
- Water temperature at state E (T_E^W: beginning of the water discharge) is equal the one at state F (T_F^W: end of water discharge).
- State F is divided into two sub states: F^- (end of water discharge) and F^+(beginning of the water injection).
- Pumped water volume is equal to air volume (V_B) introduced into the compression chamber.

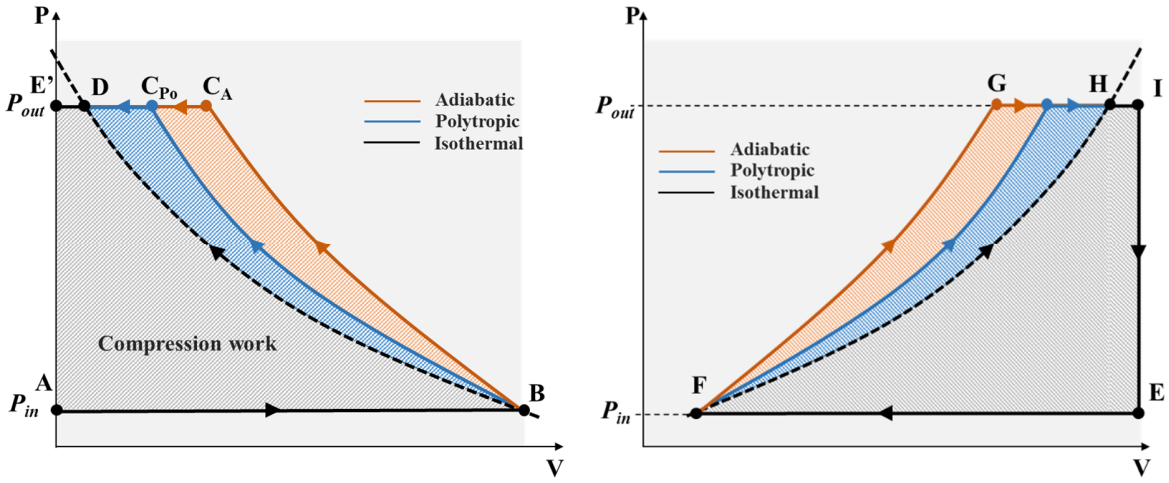

Figure 11: PV diagram of the air (left) and water (right) compression cycle

3.2.2 Analytical model of liquid piston compressor

Air energy conservation

The air intake phase energy conservation equation is described as follows:

$$\frac{dU}{dt} = \dot{m}_{AB} h_{AB} + \dot{Q}_{AB} - P\frac{dV}{dt} \tag{20}$$

By replacing the internal energy, enthalpy and air-water heat transfer rate by their expressions, Eq.(20) can be written as:

$$\dot{m}_{AB} c_p \, t \, \frac{dT}{dt} + \left(\dot{m}_{AB} c_p + he_{AB} \, S_{tu}(t)\right) T(t) = \dot{m}_{AB} c_p T_A + he_{AB} \, S_{tu}(t) T_E^w \quad (21)$$

With the air water exchange surface $S_{tu}(t)$ calculated as follow:

$$S_{tu}(t) = \frac{4}{D_{tu}} \frac{\pi D_{tu}^2}{4} L(t) \, nt = \pi \, D_{tu} \, nt \, a \, t \quad (22)$$

Where D_{tu} is the tube diameter, $L(t) = a \, t$ is the air active column length where a is a constant and t is the operational time; nt is the number of the tubes inside the compression/expansion chamber used to form the integrated heat exchanger. Based on solving Eq.*(21)* with analytical approach, the air temperature expression during air suction phase is written as follows:

$$T(t) = T_F^w + \frac{\tau}{t} \left(T_A - T_E^w\right) \left(1 - e^{-t/\tau}\right) \quad (23)$$

In this study, the air suction phase time is equal to half the air compression cycle time as considered by Lemofouet [21]. The air temperature at state B is found to be:

$$T_B = T_F^w + \frac{\tau}{\frac{t_{cy}}{2}} \left(T_A - T_E^w\right) \left(1 - e^{-\frac{t_{cy}}{2}/\tau}\right) \quad (24)$$

Similarly, based on the energy equation for the air discharge phase (C_{Po} →D), the air temperature at state D is found to be:

$$T_D = T_G^w + \left(T_{C_{Po}} - T_G^w\right) e^{-NTU \left(\frac{1}{2} - \frac{t_C}{tcy}\right)} \quad (25)$$

With $NTU = \frac{nt \, he_{AB} \, D_{tu} \, \pi \, L_0}{\dot{m}_{AB} \, c_p}$.

- **Air mass conservation**

The air mass flow rate sucked during a compression cycle is given by the next equation:

$$\dot{m}_{AB} = \frac{V_B(\frac{t_{cy}}{2}) \, \rho}{t_{cy}/2} \quad (26)$$

Where the displacement volume in all the compression chamber is given by:

$$V_B = nt\ \frac{\pi\ D_{tu}^2}{4} L(\frac{t_{cy}}{2}) \tag{27}$$

The volume at the end of the compression phase (V_C) depends on the aspirated air volume (V_B) and the polytropic index (n_c). It will be shown later in Eq. (34) that the polytropic index depends on the air temperature at the end of the compression phase. At the state C, the compressed air volume is calculated as follows:

$$V_C\ =\ \left(\frac{P_{in}}{P_{out}}\right)^{\frac{1}{n_c}} V_B \tag{28}$$

- **Water energy conservation**

Describing the five phases (E→F→G→H→I→E), the water energy balance equation can be described as follows (assuming phase H→E as adiabatic process):

$$\dot{m}^w(h_{EF}^w - h_{FG}^w - h_{GH}^w)t_{cy} = \left(\dot{W}_{tot}\right)_c + \dot{Q}_{EF} + \dot{Q}_{FG} + \dot{Q}_{GH} + \dot{Q}_{HI} \tag{29}$$

To calculate the outlet water temperature it is necessary to express its enthalpy as a function of its pressure and its temperature, by separating the internal energy from the mechanical content of the enthalpy (neglecting the kinetic and gravitational energies):

$$h^w =\ C_w T + \frac{P}{\rho^w} \tag{30}$$

To simplify the problem, the transfer of mechanical energy is supposed to be isothermal; In this case, the outlet water temperature is given by the following expression:

$$T_{F^-}^w =\ T_{in}^w - \frac{\dot{Q}_{(tot)_c}}{c_w \dot{m}^w} = T_{F^+}^w - \frac{\dot{Q}_{EF} + \dot{Q}_{FG} + \dot{Q}_{GH} + \dot{Q}_{HI}}{c_w \dot{m}^w} \tag{31}$$

- **Complementary equations**

The total air compression work rate is defined by the following equation:

$$\dot{W}_{(tot)_c} = (-P_{in}V_B + \frac{1}{n_c - 1}(P_{out}V_{C_{Po}} - P_{in}V_B) + P_{out}V_{C_{Po}})\frac{1}{\eta_{pol}\ t_{cy}} \tag{32}$$

And the total heat transfer exchanged between water and air is given by the following:

$$\dot{Q}_{(tot)_c} = \dot{m}_{AB}\ c_p\ (T_{\mathrm{B}} - T_A) + he_{BC_{Po}}\left(\frac{V_B + V_{C_{Po}}}{0{,}5\ D_{tu}}\right)\left(T_{F^+}^w - \left(\frac{T_{C_{Po}} + T_B}{2}\right)\right) + \dot{m}_{C_{Po}D}\ c_p\ (T_{\mathrm{D}} - T_{C_{Po}}) \tag{33}$$

Many scientific researchers studied and analyzed the heat transfer coefficient for the liquid piston during the air compression phase. Van de Ven and Li [25] used a fully developed pipe flow

analysis to model the liquid piston system in order to roughly estimate the heat transfer between the air and the liquid. The studied heat transfer coefficient was between 50-350 $W.m^{-2}.K^{-1}$. Odukomaiya [24] developed GLIDES (Ground-Level Integrated Diverse Energy Storage) technology which is based on liquid piston compression/expansion. In his work, Odukomaiya conducted numerical model calibrated by his collected experimental data. The gas-liquid heat transfer coefficient was found to be in the range of 200-500 $W.m^{-2}.K^{-1}$. These later heat transfer coefficient ranges are used in this study. The polytropic index of the compression phase is calculated from the following:

$$n_c = ln\frac{P_{in}}{P_{out}} \Big/ ln\frac{T_{C_{Po}}}{T_B} + ln\frac{P_{in}}{P_{out}} \tag{34}$$

3.2.3 Analytical model of liquid piston expander

The mass conservation and the complementary equations used for the liquid piston expander model are similar to those used for the compression mode. The different states of air and water during the air expansion process are shown in Figure 12.

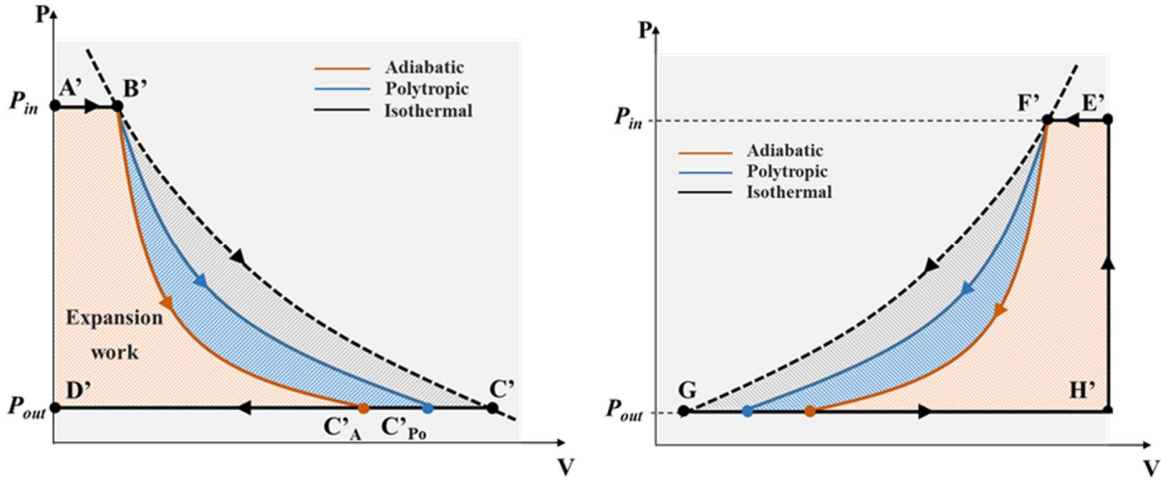

Figure 12: PV diagram of the air (left) and water (right) expansion cycle

- **Air energy conservation**

Equation (20) is also applicable for the compressed air suction phase (A'→B') and the air temperature at state B' (end of air suction phase) is:

$$T_{B\prime} = T_{out}^{w} + \frac{\tau}{t}\left(T_{A\prime} - T_{out}^{w}\right)\left(1 - e^{-t/\tau}\right) = T_{E\prime}^{w} + \frac{\tau}{t}\left(T_{A\prime} - T_{E\prime}^{w}\right)\left(1 - e^{-t/\tau}\right) \quad (35)$$

The air discharge phase is also similar to that developed for the compression mode. Therefore, the air temperature at state D' (end of air discharge phase):

$$T_{\mathrm{D}\prime} = T_{in}^{w} + \left(T_{C_{Po}^{\prime}} - T_{in}^{w}\right) e^{\frac{-NTU}{2}} = T_{\left(G_{Po}^{\prime}\right)^{+}}^{w} + \left(T_{C_{Po}^{\prime}} - T_{\left(G_{Po}^{\prime}\right)^{+}}^{w}\right) e^{\frac{-VR_t\, NTU}{2}} \quad (36)$$

With $NTU = \frac{nt\, he_{AB}\, D_{tu}\, \pi\, L_0}{\dot{m}_{AB}\, c_p}$, and $(VR_t \frac{t_{cy}}{2})$ is the compressed air introduction time into the expander. VR_t is the volume ratio ($VR_t = \frac{V_{B\prime}}{V_{C_{Po}^{\prime}}}$).

- **Air mass conservation**

The compressed air mass flow rate introduced into the expander is expressed as follows:

$$\dot{m}_{A\prime B\prime} = \frac{V_{B\prime}\,\rho}{t_{cy}} \quad (37)$$

With expanded air volume calculated from the following equation:

$$V_{C_{Po}^{\prime}} = \left(\frac{P_{in}}{P_{out}}\right)^{\frac{1}{n_t}} V_{B\prime} \quad (38)$$

- **Water energy conservation**

Total heat transfer calculated in Eq. (42) which is based on the air temperature evolution through the air expansion cycle, is considered equal of the total heat transfer calculated with water temperature evolution during the air expansion cycle. Therefore, the outlet water temperature of the expansion chamber is calculated as follows:

$$T_{\left(G_{Po}^{\prime}\right)^{-}}^{w} = T_{in}^{w} - \frac{\dot{Q}_{(tot)_t}}{c_w \dot{m}^w} = T_{\left(G_{Po}^{\prime}\right)^{+}}^{w} - \frac{\dot{Q}_{E\prime F\prime} + \dot{Q}_{F\prime G\prime} + \dot{Q}_{G\prime H\prime}}{c_w \dot{m}^w} \quad (39)$$

- **Water mass conservation**

Inlet water mass flow rate is assumed equal the outlet water mass flow rate and calculated from the following equation:

$$\dot{m}_{out}^{w} = \dot{m}_{in}^{w} = \frac{V_{C_{Po}^{\prime}} \rho_w}{t_{cy}} \quad (40)$$

- **Complementary equations**

The total air expansion work rate is defined as follows:

$$\dot{W}_{(tot)_t} = \eta_{po}(-P_{in}V_{B'} + \left(\frac{1}{n_t - 1}(P_{out}V_{C_{Po}} - P_{in}V_{B'})\right) + P_{out}V_{C'_{Po}})\frac{1}{t_{cy}} \quad (41)$$

The total heat transfer exchanged between water and air during air expansion cycle is given by the following equation:

$$\dot{Q}_{(tot)_t} = \dot{m}_{A'B'}\, c_p\, (T_{B'} - T_{A'}) + he_{B'C'_{Po}}\left(\frac{V_{B'} + V_{C'_{Po}}}{0{,}5\, D_{tu}}\right)\left(T^{w}_{E'} - \left(\frac{T_{C'_{Po}} + T_{B'}}{2}\right)\right) + \dot{m}_{C'_{Po}D'}\, c_p\, \left(T_{D'} - T_{C'_{Po}}\right) \quad (42)$$

The polytropic index for the air expansion phase is given by the following equation:

$$n_t = ln\frac{P_{in}}{P_{out}} \Big/ ln\frac{T_{C'_{Po}}}{T_{B'}} + ln\frac{P_{in}}{P_{out}} \quad (43)$$

4. Numerical resolution

All the numerical compressor and expander models detailed above are coded in MATLAB based on multiple iterative loops and multiple convergence conditions. In the mechanical piston case, three iterative loops are used for each model where polytropic index, outlet absolute humidity and outlet water temperature are chosen to be the convergence parameters. Liquid piston numerical code, in turn, is based on two main iterative loops using the compressor/expander outlet water temperature ($T^{w}_{F^-}$, $T^{w}_{G'_{Po}}$) and the air temperature at the end of the compression/expansion phase ($T_{C_{Po}}, T_{C'_{Po}}$) as convergence parameters (Figure 11). Dichotomy method is used specially for the air temperature at the end of the compression/expansion phase calculation where it is limited between the air temperature at the beginning of the compression phase (T_B)/expansion phase ($T_{B'}$) and the adiabatic air temperature at the end of the compression phase (T_{C_A})/expansion phase ($T_{C'_A}$).

5. Results and discussion

5.1 Mechanical piston air compressor/expander

Three air compressors/expanders stages detailed above are considered in the next section. Table 2 lists the compressor model fixed and initialized inputs. Parallel cooling method is adopted for this air compressors architecture whereas water mass flow equals to 0.0872 kg/s at 10 °C is injected at each compressor inlet. Three indicators were selected in order to analyze and validate the

compressor/expander model: heat transfer coefficient, mass loading (the mass of water spray over the mass of sucked air) and droplet diameter.

Table 2: Numerical compressor model inputs

	Low pressure	Middle pressure	High pressure
Pressure range (bar)	1 → 6	6 → 36	36 → 216
Inlet air temperature (°C)	20	Outlet 1st comp.	Outlet 2nd comp.
Inlet AAH ($g_{water}/kg_{dry\ air}$)	8.9	Output first stage	Output second stage
Inlet dry air mass flow rate (kg/s)	0.01744	0.01744	0.01744
Polytropic efficiency	0.8	0.8	0.8
Inlet water droplet radius (μm)	16	16	16
Ambient air temperature (°C)	20	20	20
Residence time of the droplets in the cylinder (s)	0.02	0.02	0.02
Initialized variables			
Polytropic index	1.10	1.10	1.10
Average water temperature (°C)	25	25	25
Outlet absolute humidity ($g_{water}/kg_{dry\ air}$)	8.9	8.9	8.9

Figure 13 shows that for a fixed droplet diameter (DD = 16 μm) and mass loading (ML = 5), the outlet air temperatures for the three compressors decrease with the increase of the heat transfer coefficient. This fact is therefore responsible for the increase of the outlet water temperature of each compressor as seen in Figure 14. Heat transfer coefficient was extended to 500 $W/m^2.K$ in order to see our system performance reaction. It should be noted that after 400 $W/m^2.K$ - 450 $W/m^2.K$, the outlet air/water compressor temperature remains relatively constant. The difference of air/water temperature between the first compressor inlet and last compressor outlet is noted to be equal to 22 °C/16.5 °C for a heat transfer coefficient of 400 $W/m^2.K$. A drop of the absolute humidity is noticed (Figure 15) during the first compression process (8.9 $g_{water}/kg_{dry\ air}$ to 2.18 $g_{water}/kg_{dry\ air}$) at 100 $W/m^2.K$ which explains the important rise in air temperature for the first air compression stage based on the equation of state for humid air. By the increase of the heat transfer coefficient, the outlet air compressor temperature as well the polytropic index decrease as seen in Figure 15. The isothermal efficiency is defined as the isothermal compression work divided by the real work. The increase of heat transfer coefficient leads to a decrease of compensated total work rate which increases the isothermal efficiency as noticed in Figure 15.

Series cooling method was also investigated, for the same droplet diameters and mass loading. At 100 W/m^2.K water that entered the first compressor at 10 °C was seen to leave the third one with a temperature of 40.66 °C. In this cooling method and while increasing the heat transfer coefficient, air temperature was noticed to have higher degrees than parallel cooling method.

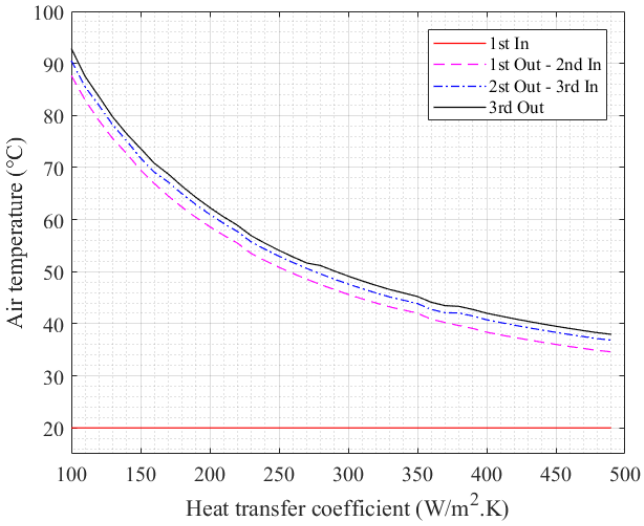

Figure 13: Air temperature going through the three air stage compressors as a function of heat transfer coefficient

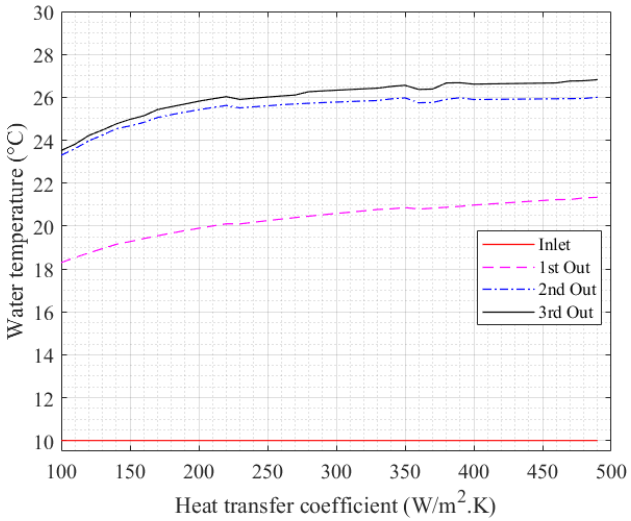

Figure 14: Water temperature going through the three air stage compressors as a function of heat transfer coefficient

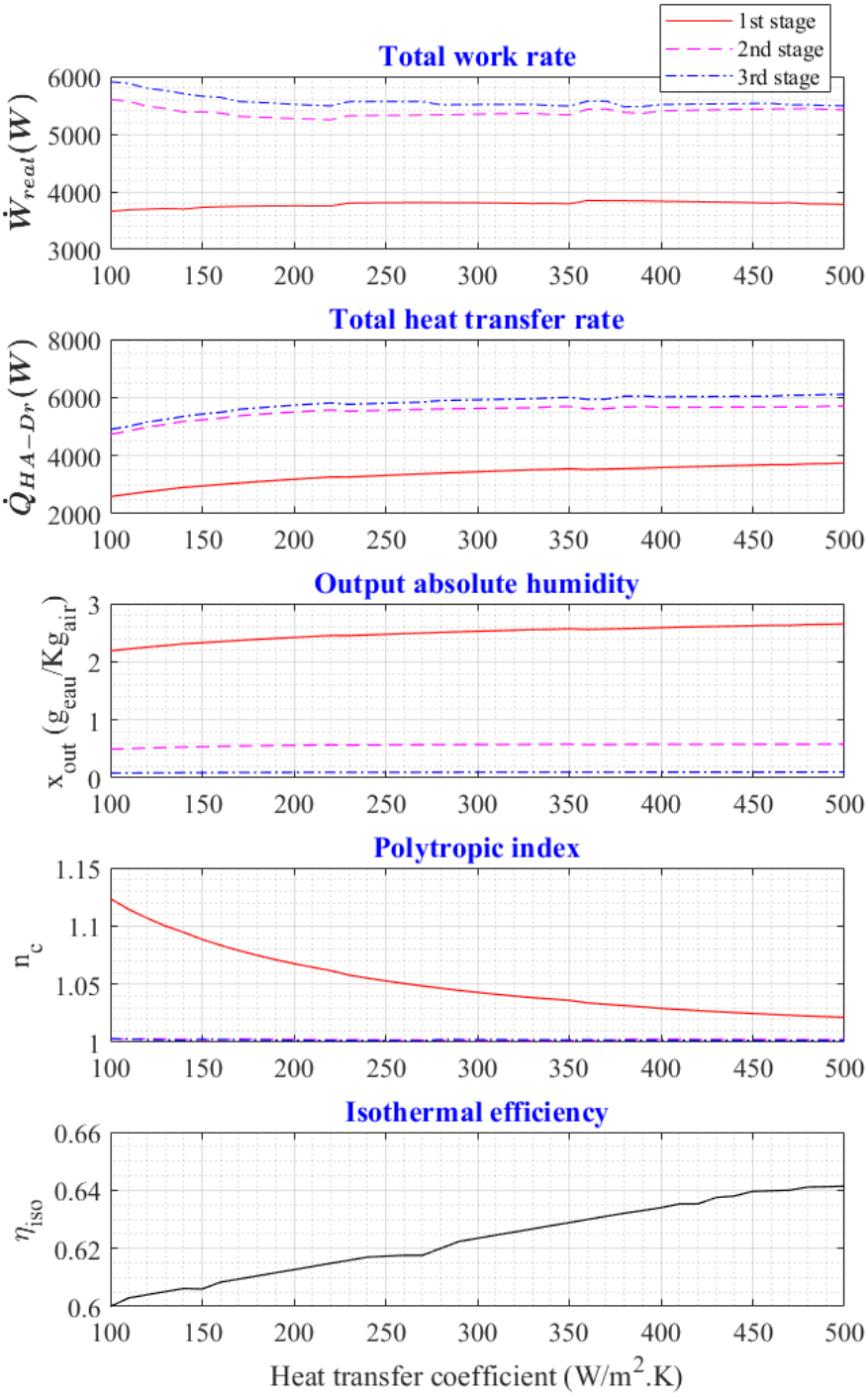

Figure 15: Several outlet parameters as function of the heat transfer coefficient. The legend of the first figure at the top has to be considered for the other figures below

Figure 16 and Figure 17 showed the results of water droplet size influence during the compression phase taking into account a fixed heat transfer coefficient (HTC = 400 W/m^2.K) and mass loading (ML = 5). The droplet diameter used in this study is in the same range used in Qin

and Loth work [18] (16 µm – 36 µm) which is reasonably achievable by most spray nozzles. As droplet diameter increases, the injected surface becomes lower and therefore decreases the heat transfer between the humid air and cold water injected. These results show a perfect match with the experimental work done by Qin and Loth [18] where they investigated the efficiency of the air compression with the water injection.

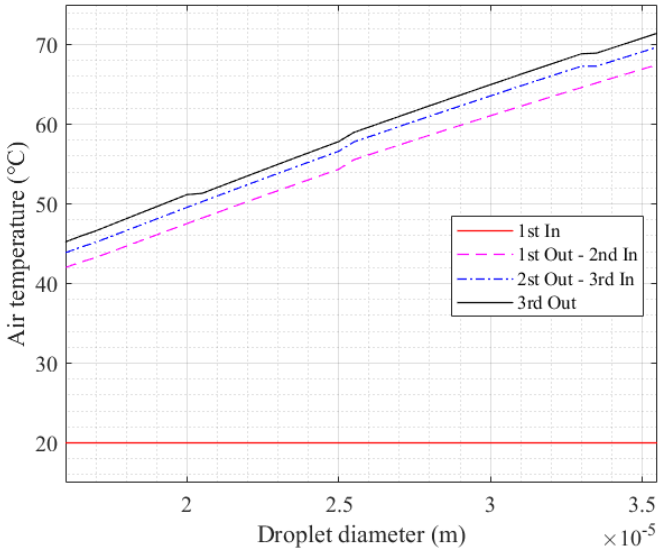

Figure 16: Air temperature as a function of water droplet diameter

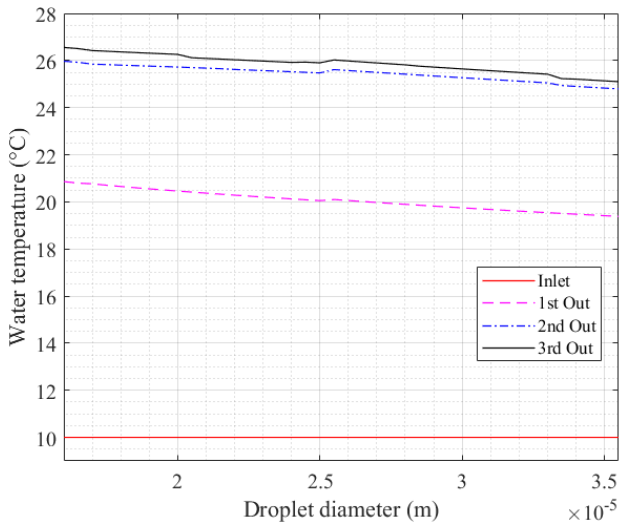

Figure 17: Water temperature as a function of water droplet diameter

The mass loading variation impact is seen in Figure 18 and Figure 19 while fixing the heat transfer coefficient (HTC = 400 W/m^2.K) and the droplet diameter (DD = 16 µm). The higher the water mass flow rate the lower the compressor outlet air/water temperature and the closer to an

isothermal air compression process. This fact was also observed by Qin and Loth in their investigation of the droplet spray solution for achieving high heat transfer during air compression [18].

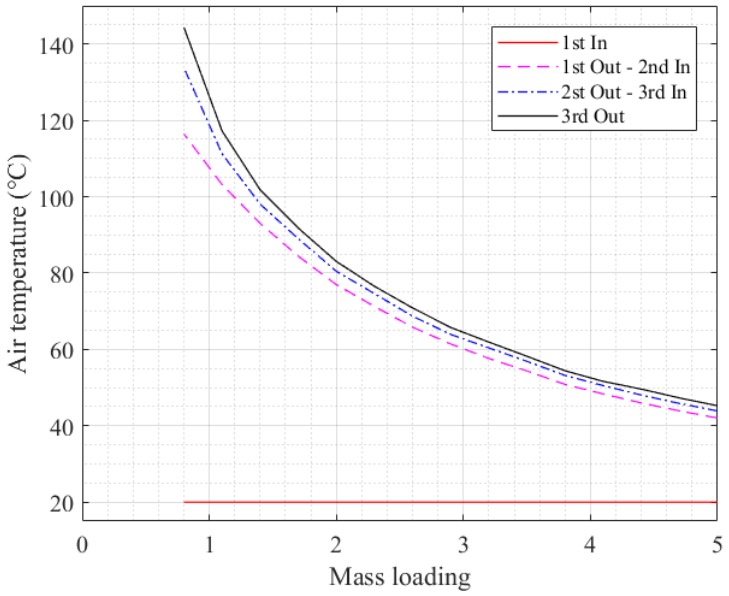

Figure 18: Air temperature as a function of mass loading

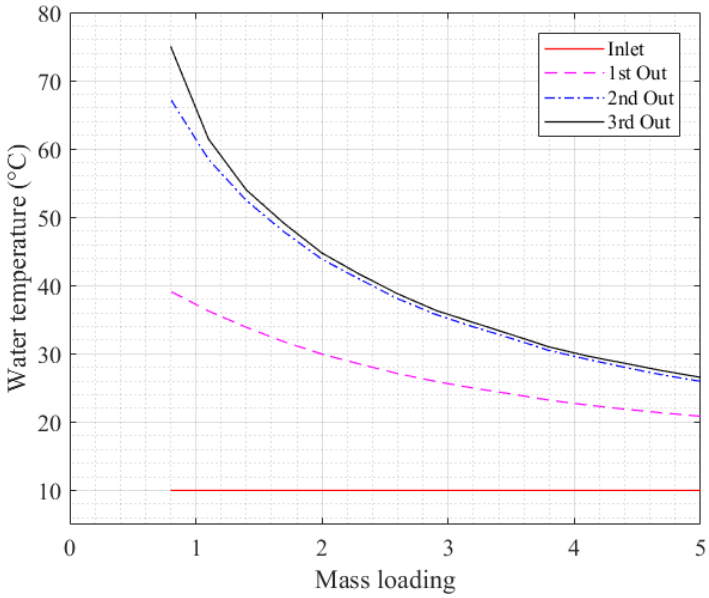

Figure 19: Water temperature as a function of mass loading

The fixed input parameters showed in Table 2 are similar for the expander numerical model. In this case, compressed air stored at 216 bar with a temperature of 20°C, is expanded through three

air expanders (216 bar →1 bar). Similar to the compressor model, hot water is injected separately in each of the three expanders with the same inlet water temperature (60 °C) in order to heat the compressed air during the expanding process. Figure 20 shows that the outlet air temperatures for the three expanders increase with the increase of the heat transfer coefficient (with DD = 16 μm and ML = 5). This fact indicates that the more air/water heat transfer, the higher air temperature and the lower water temperature leaving the expander (Figure 21). It should also be pointed that the outlet absolute humidity is increasing while passing through expander stages. This fact is explained by the relation between the absolute humidity and the outlet air pressure described in Eq. (5).

Series heating method is also investigated for the expander case. At the outlet of the expander the air was found to be warmer than the parallel heating method especially for the third air stage expander but after 150 W/m^2.K the heating method was shown a minor impact.

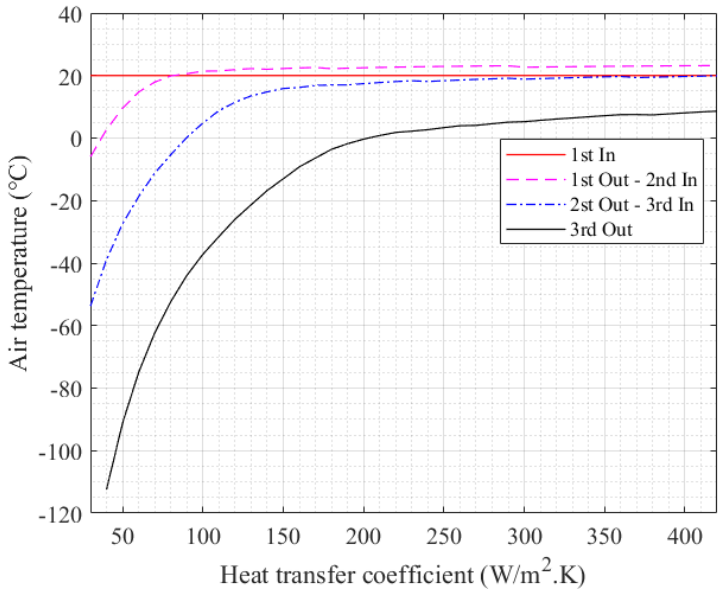

Figure 20: Air temperature going through the three air stage expanders as a function of heat transfer coefficient

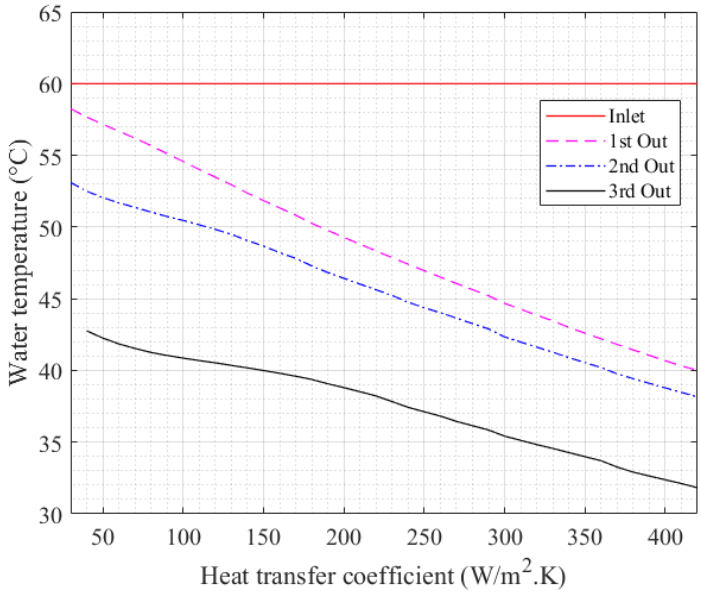

Figure 21: Water temperature going through the three air stage expanders as a function of heat transfer coefficient

Like in the compressor case, the droplet diameter influence on the air and water temperature going through the three air stage expanders is shown Figure 22 and Figure 23. It was noticed that increasing the droplet diameter (with HTC = 250 W/m^2.K and ML = 5) implies a significant decrease of the air temperature especially for the second and third air stage expander while an increase of the water temperature is noticed. This fact can be justified based on the Eq 3.9 where the increase of the droplet diameter results in a decrease of the droplet numbers injected in the expander and therefore a decrease in the air/water heat transfer.

The mass loading variation impact for a fixed heat transfer coefficient (HTC = 250 W/m^2.K) and droplet diameter (DD = 16 µm) is presented in Figure 24 and Figure 25. The higher the water mass flow rate the higher the expander outlet air/water temperature. Equations Eq. (5) and Eq. (9) justify the relations between the outlet water temperature, absolute humidity and the outlet air temperature.

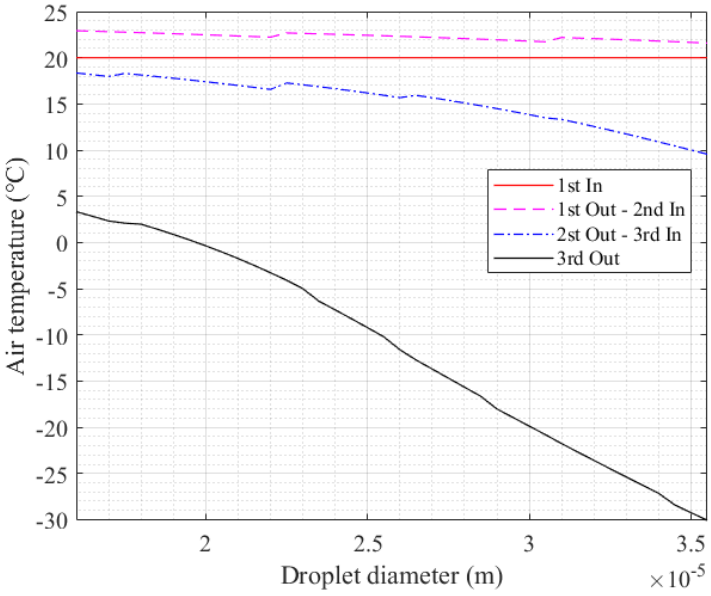

Figure 22: Air temperature as a function of water droplet diameter

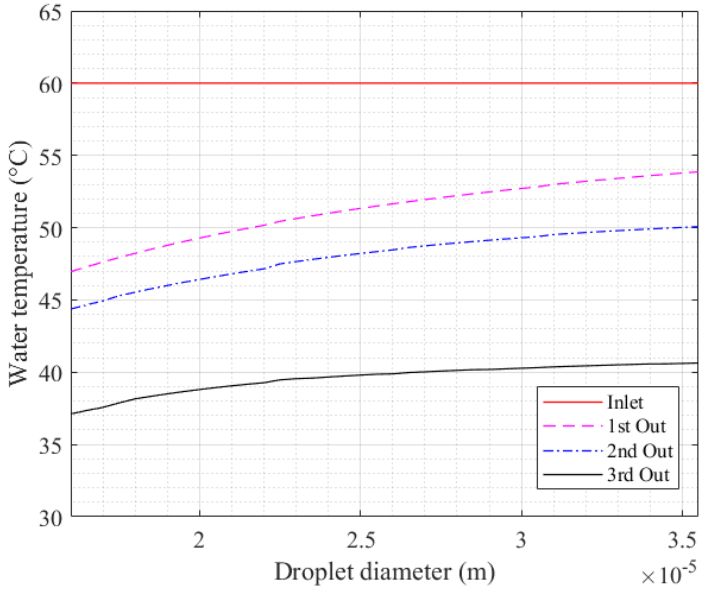

Figure 23: Water temperature as a function of water droplet diameter

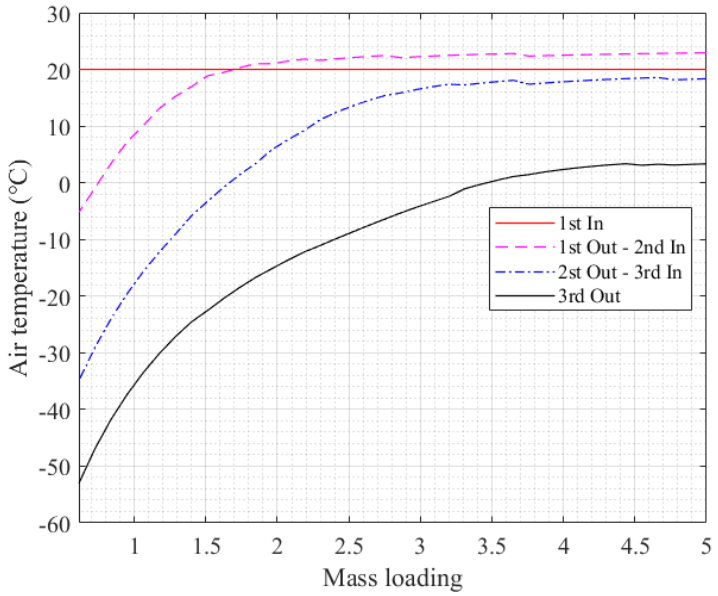

Figure 24: Air temperature as a function of mass loading

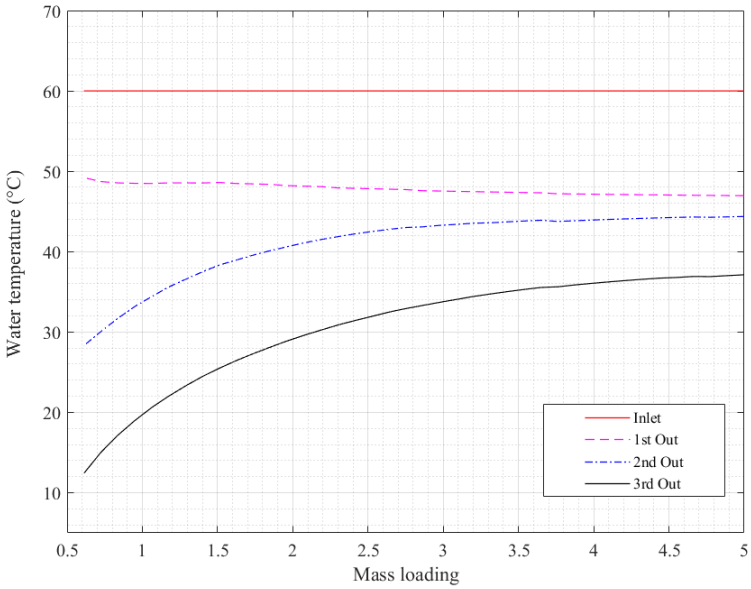

Figure 25: Water temperature as a function of mass loading

5.2 Liquid piston air compressor/expander

The liquid piston compressor/expander numerical model is inspired from the liquid piston compressor/expander experimental system designed and published by Enairys Powertech [21]. Therefore, a two stages of liquid piston air compressors/expanders (High and low pressure) are chosen to be simulated. Table 3 lists the data inputs required for the liquid piston compressor and expander fixed by Enairys Powertech [21], [22].

Table 3: Experimental liquid piston compressor model inputs

	Low pressure	High pressure
Pressure range (bar)	10 → 40	40 → 160
Compression ratio	4	4
Inlet air temperature (°C)	24	Outlet 1st comp
Inlet water temperature (°C)	23	23
Cylinder volume (L)	62.8	15.7
Cylinder height (m)	0.5	0.5
Cylinder diameter (m)	0.4	0.2
Tube diameter (mm)	2	1
Cycle time (s)	20	20

Based on the input data fixed by Enairys Powertech, the air mass flow rate sucked by the liquid piston compressor is equal to 0.01469 kg/s. Like the mechanical piston case, three indicators were chosen to study their influence on the concern technology: heat transfer coefficient, tube diameter and air mass flow rate. It should be mentioned that during the air intake phase, water that underwent a previous compression cycle is pumped out of the compressor.

It is noticed from Figure 26 that the water leaves the compressor with a small increase in temperature. The air temperature is seen to be dropped while air is introduced in the chamber (Phase A→B) where at the same time water temperature is increased. For instance, at 5 $W.m^{-2}.K^{-1}$ the first and second stage water temperature difference is 0.4 and 1.2 °C respectively. The highest air temperature at the end of the compression phase is equal to 47.2 °C and 61.6 °C for the 1st and 2nd stage respectively (at 5 $W.m^{-2}.K^{-1}$). This temperature ($T_{C_{Po}}$) is rapidly decreased with the increase of the heat transfer coefficient to stabilize for 80 $W.m^{-2}.K^{-1}$ around 24.5 °C and 25.7 °C for each stage compressor. During discharge phase, water is pumped at 23 °C and therefore compressed air is pushed out of the chamber. This air/water indirect contact justifies the air temperature drop while leaving the cylinder (at 80 $W.m^{-2}.K^{-1}$ compressed air leaving the first compressor dropped from 24.5 °C to 24.3 °C and from 25.7 °C to 25.5 °C for the second). These results show a fair agreement with those presented in Enairys Powertech work [21], where the average outlet air temperature of the first stage air compressor scored an increase of 1 °C and 0.2 °C for water leaving the same compressor. Figure 27 shows consistent values for the total work rate, the total heat transfer rate and the polytropic index while varying the heat transfer coefficient. In fact as the heat transfer coefficient increases the air/water heat transfer increases which leads to a decrease in the total compensated work and therefore the polytropic index converged to unity and the isothermal compression efficiency increases.

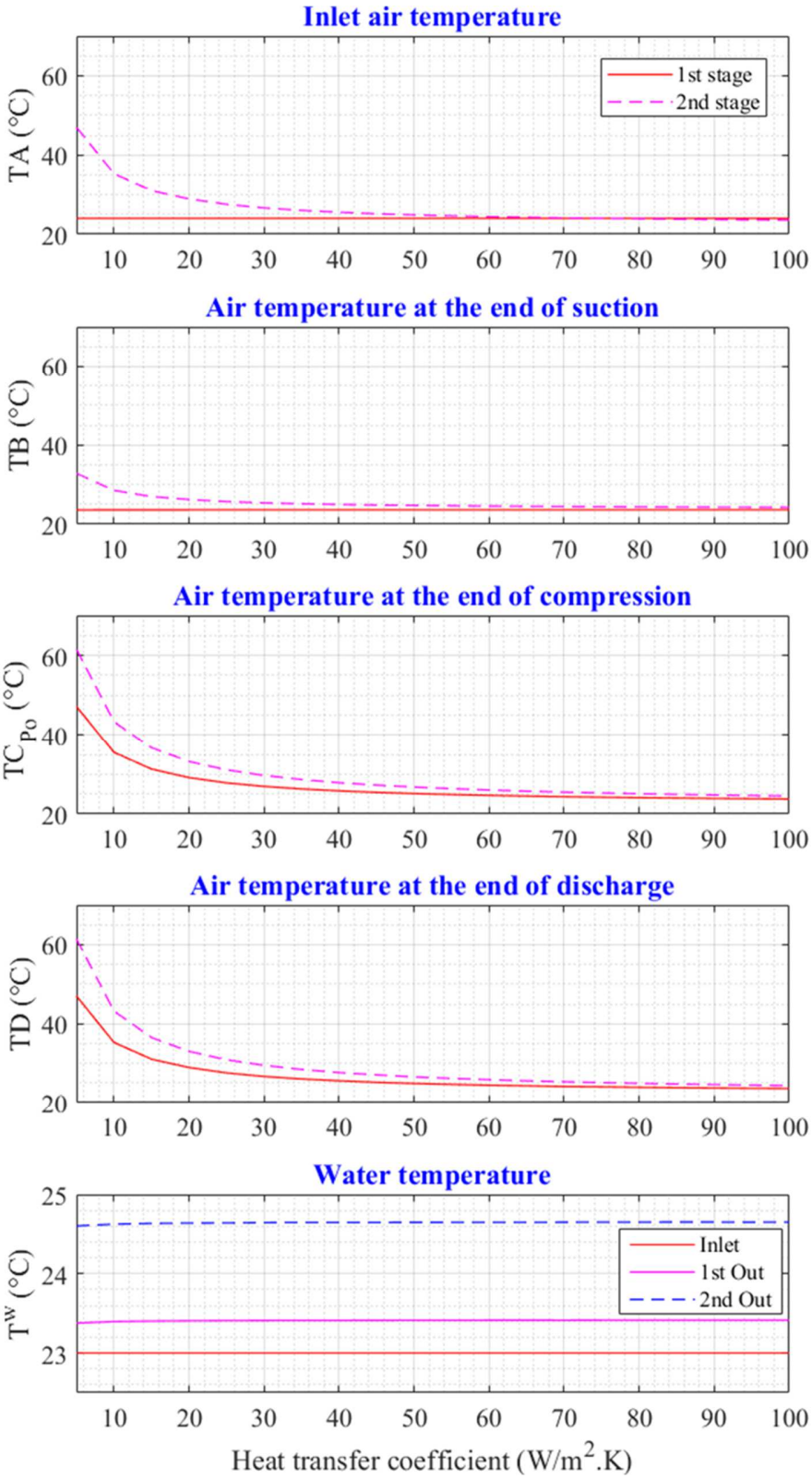

Figure 26: Air/Water temperature at different air compression states function of the heat transfer coefficient. The legend of the first figure at the top has to be considered for the other figures below.

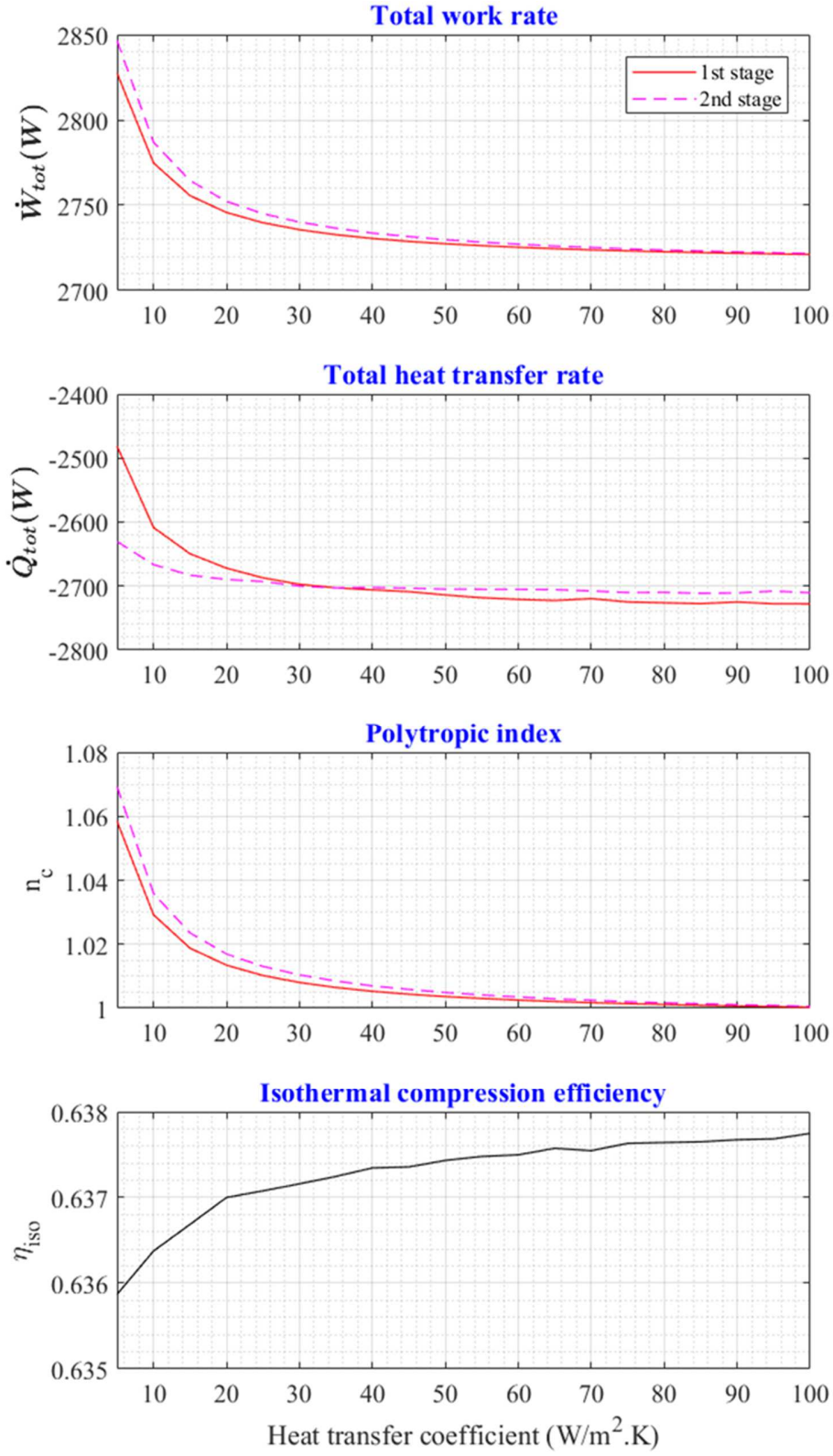

Figure 27: Several liquid piston compressor model outputs function of the heat transfer coefficient

Figure 28 shows the impact of the 2nd stage air compressor tube diameter (varying from 1 mm to 10 mm) on the air and water temperature at the end of compression and discharge phase respectively. With a fixed HTC equal to 80 $W.m^{-2}.K^{-1}$ and air mass flow rate at 0.01469 kg/s, the air temperature at the end of the compression is increased. This fact is justified by the relation between the tube diameter and their numbers (inversely proportional based on Eq. (22)) which means that increasing the diameter reduces the tube numbers and as a result reduces air/water heat transfer.

Figure 29 presents the influence of the air mass flow rate (varying from 0.01469 kg/s to 0.29 kg/s) on the water and air temperatures with a fixed tube diameter (TD) for second compressor at 1 mm and HTC at 80 $W.m^{-2}.K^{-1}$. The higher the air mass flow rate for the same water mass flow rate, the higher the air temperature at the end of the air compression phase. From above results, tube diameter and air mass flow rate have a negligible impact on water temperature.

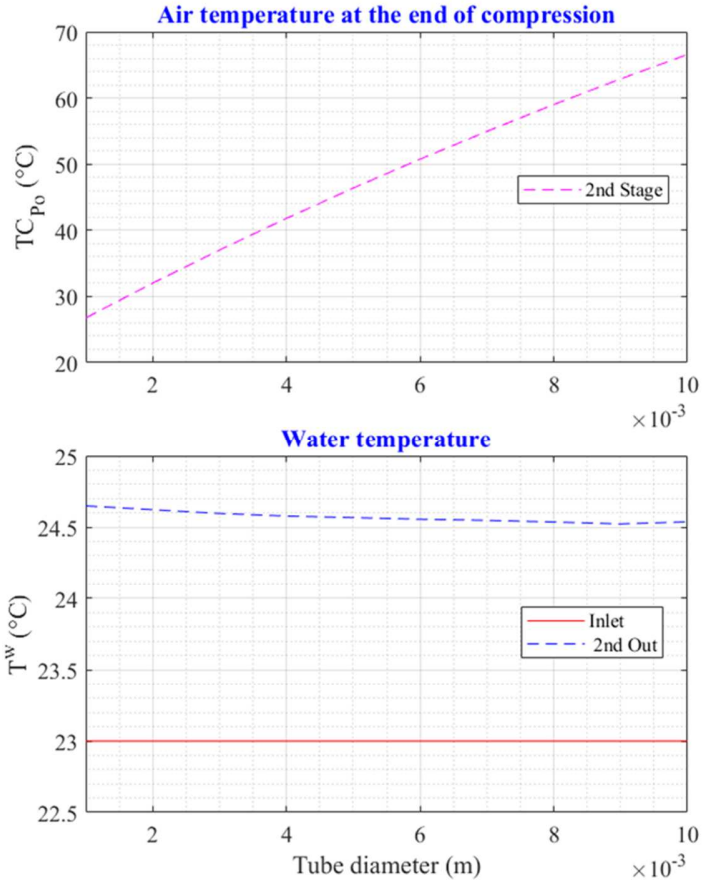

Figure 28: Air/water temperature at the end of compression function of 2nd stage compressor tube diameter

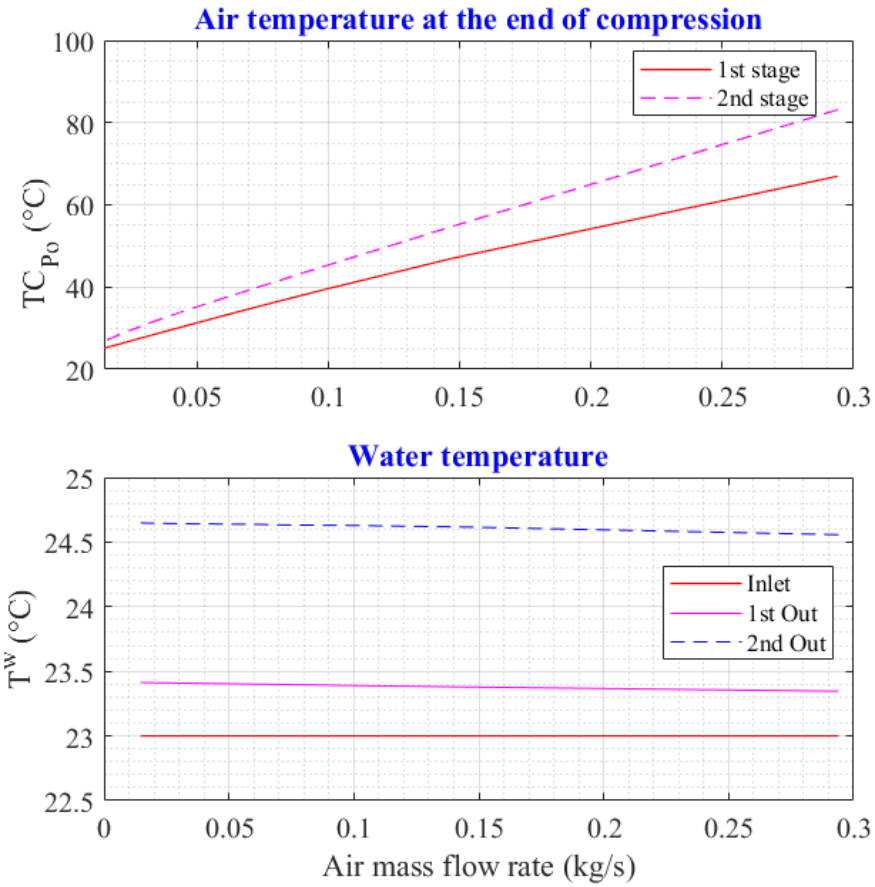

Figure 29: Air and water temperature at the end of compression function of air mass flow rate

The expander numerical model inputs are similar to the ones listed in Table 3. In this case the first stage air expansion is the high pressure stage followed by the low pressure stage. Inlet air temperature is fixed at 20 °C with 23 °C for expander inlet water. Based on Figure 30 the heat transfer coefficient has a fair influence on air temperature at different states during the air expansion process and minor influence on water temperature. Noting that in this case the air mass flow rate is fixed at 0.01469 kg/s for 1 mm for the 1st stage and 2 mm for the 2nd stage air expander. This influence is clearly seen for the air temperature at the end of the expansion especially from 5 $W.m^{-2}.K^{-1}$ to 40 $W.m^{-2}.K^{-1}$. It can be seen that during compressed air suction phase, its temperature rises due to indirect contact with warm water leaving the expander. Same approach is noticed for the air discharge phase where the warm injected water is in indirect contact with the air. Similar to the observations noticed for the compressor model, Figure 31 shows that the increase of the 2nd stage air expander tube diameter deteriorates the air temperature

at the end of the expansion while fixing the HTC at 80 $W.m^{-2}.K^{-1}$ and 0.01469 kg/s as mass flow rate.

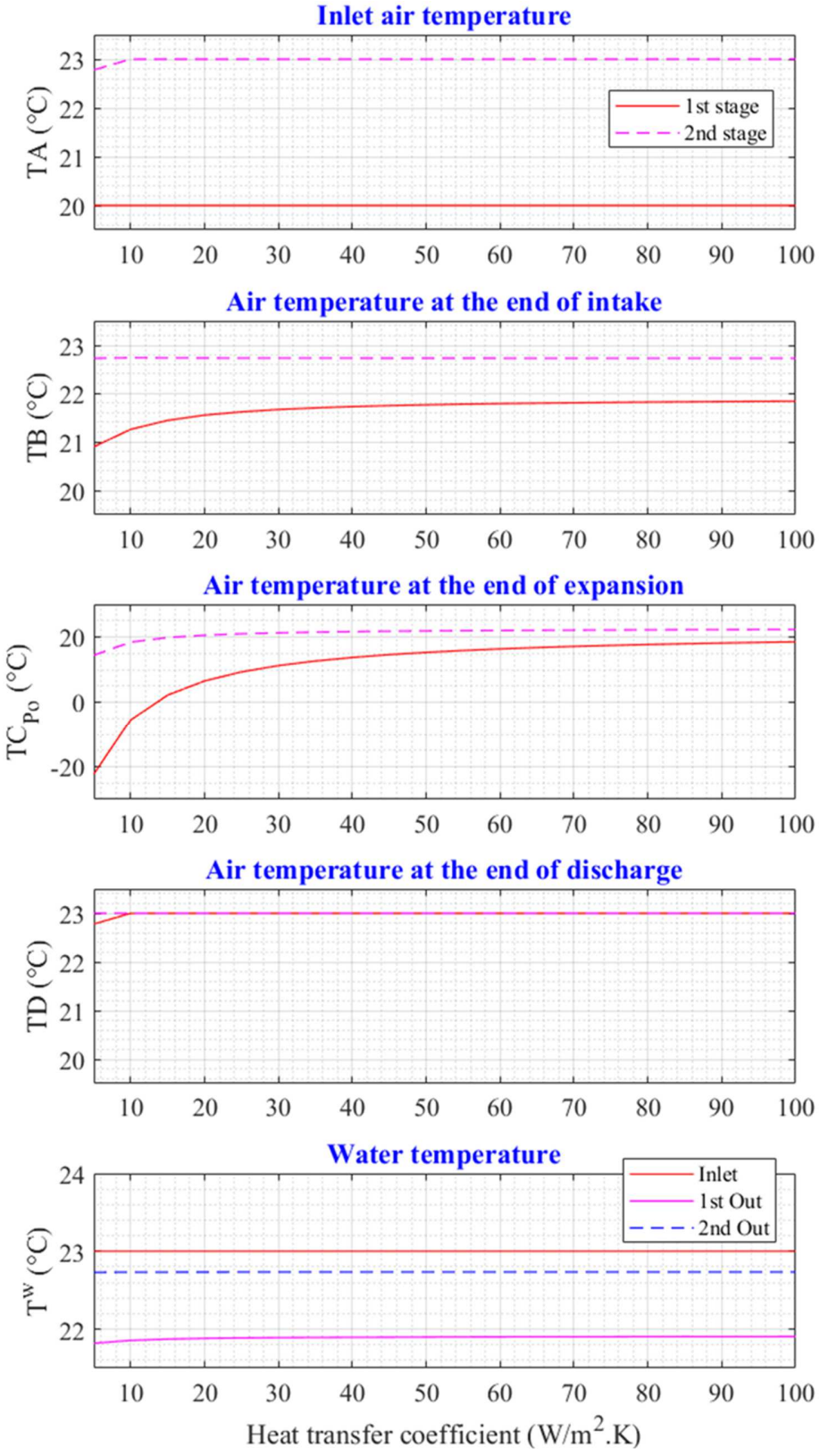

Figure 30: Air/Water temperature at different air expansion states function of the heat transfer coefficient

This fact is due the drop in the heat transfer between air and water. The third parameter influence to analyze is the air mass flow rate variation with fixed TD (2 mm) and HTC (80 $W.m^{-2}.K^{-1}$). Figure 32 highlights the impact of introducing more compressed air in the expander for the same water flow. This impact affects heavily the air temperature at the end of the expansion phase while in contrary water seems not heavily impacted.

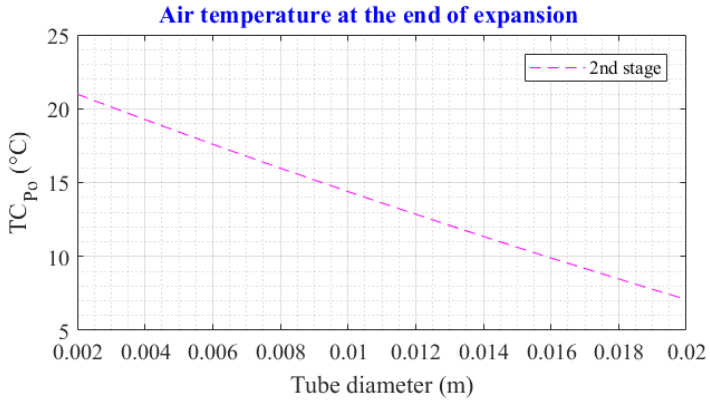

Figure 31: Air temperature at the end of expansion function of 2nd stage expander tube diameter

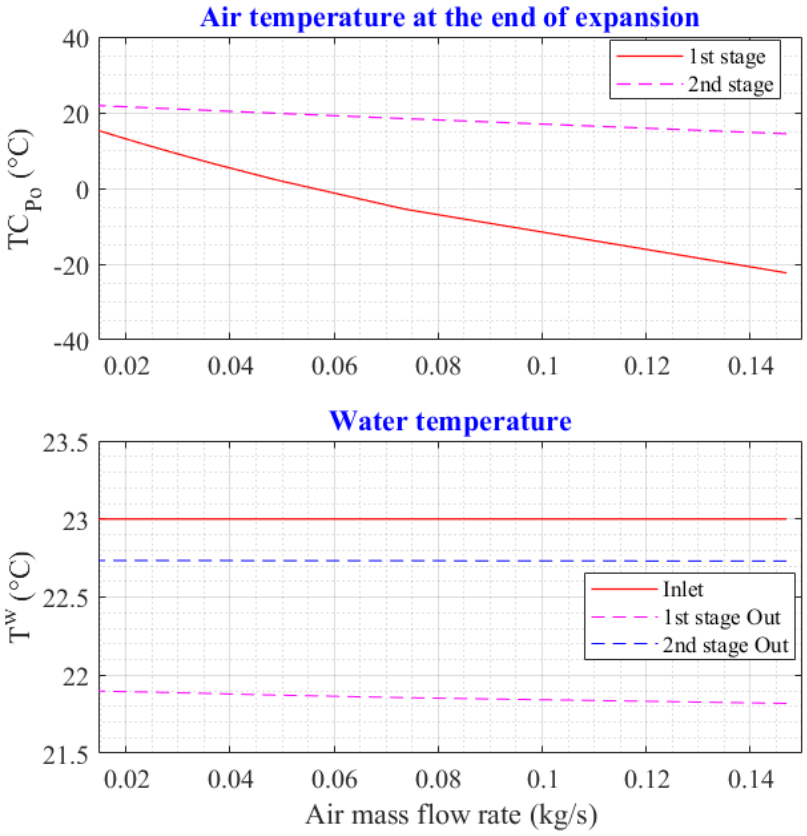

Figure 32: Air and water temperature at the end of expansion function of air mass flow rate

6. Conclusion

A quasi-isothermal compressor and expander developed by LightSail Energy (mechanical piston compressor/expander with water injection) and Enairys Powertech (liquid piston compressor/expander with integrated heat exchanger) were investigated for the first time in this article. Several scientific works that describe similar technologies were used in this study. Detailed analytical simplified models were presented for each technology. It was notably highlighted the influence of the heat transfer coefficient, heat transfer exchange surface and mass loading on the compressor/expander operation with tracing the behavior of the system outputs (air/water temperature, humidity, work rate, heat transfer rate,…). It was evidenced that the mechanical piston compressor is more favorable for the production of hot water (or cold in case of expansion) than the liquid piston technology that presented a strong isothermal compression and expansion process. Furthermore, the analytical models developed in this article were used in Dib's thesis work, where a global numerical sizing tool was elaborated in order to simulate a small-scale compressed air energy storage system [26].

Appendix (Mass transfer between air and water droplet)

Mass transfer between the air and the injected water during compression/expansion will be guided by the difference of water vapor pressure contained in the air and in the vicinity of the water droplets where the partial water vapor pressure ($P^{wv}_{partial}$) is equal to the saturated water vapor pressure (P^{wv}_{SAT}) at the temperature of water. This partial water vapor pressure in the vicinity of the water droplet will play a big role to push away or to attract the water vapor contained in the air.

During the compression phase, the air temperature is higher than that of the cold injected water. The water vapor contained in the air will migrate towards to or escape from the water droplet as long as the partial water vapor pressure contained in the air is higher or lower than the partial water vapor pressure in the vicinity of droplet. At the compressor outlet, it is assumed that there is no more mass transfer and in this case, the partial water vapor pressure in the air is equal to the saturated water vapor pressure at the water outlet temperature. In other words the wet temperature is equal to that of water (Figure 33).

During the expansion phase (Figure 34), the compressed air is cooler than the hot injected water. This will help to fill the air with water vapor (humidification/increase of the partial water vapor pressure in the air), until the air is saturated. In fact, the water vapor in the vicinity of droplet at water temperature have a higher pressure than the water vapor pressure in air. The mass transfer will take place from water droplet to air, until saturation.

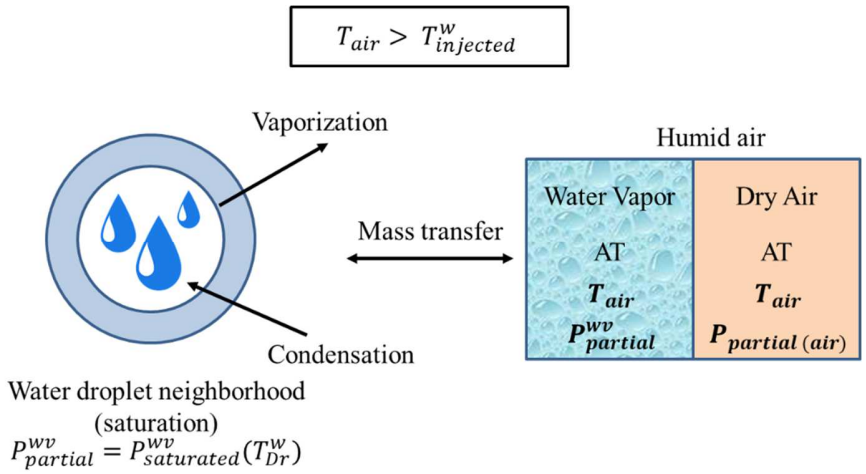

Figure 33: Mass transfer between water droplets injected inside the cylinder during compression

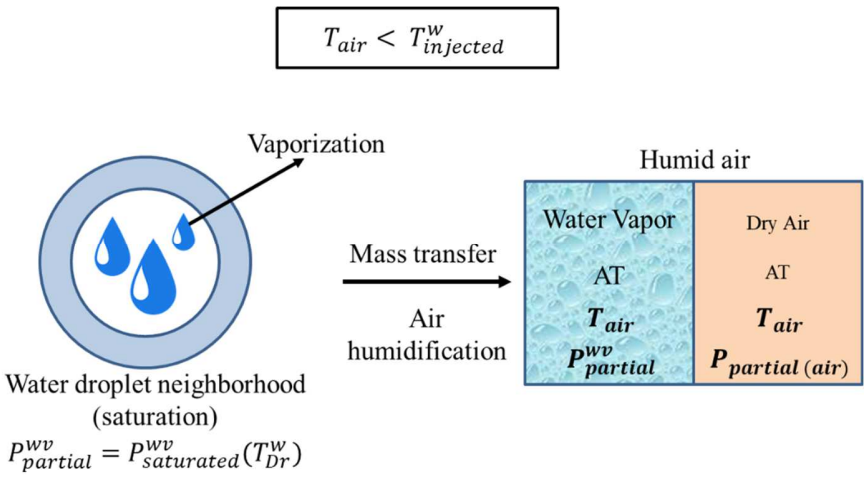

Figure 34: Mass transfer between water droplets injected inside the cylinder during expansion

Acknowledgment

This scientific research was financed by:

- ANRT (The National Association of Research and Technology) and AIA LIFE DESIGNERS (France) for the PhD grant within the framework of a CIFRE convention.

References

[1] Y. Coltier *et al.*, "Chiffres clés des énergies renouvelables - Édition 2019," pp. 1–92, 2019.

[2] Réseau de Transport d'Électricité - RTE, "Electricity report 2018," 2019.

[3] CEA, "Le stockage stationnaire de l'énergie," p. 41, 2012.

[4] G. Venkataramani and J. Wang, "A review on compressed air energy storage – A path way for smartgrid and polygeneration," *Renew. Sustain. Energy Rev.*, vol. 62, pp. 895–907, 2016.

[5] M. Budt, D. Wolf, R. Span, and J. Yan, "A review on compressed air energy storage: Basic principles, past milestones and recent developments," *Appl. Energy*, vol. 170, pp. 250–268, 2016.

[6] I.-énergie Nouvelle, "Le stockage massif de l'énergie," 2013.

[7] J. Wang, "Overview of compressed air energy storage and technology development," *Energies*, vol. 10, no. 7, p. 22, 2017.

[8] L. Chen, T. Zheng, S. Mei, and X. Xue, "Review and prospect of compressed air energy storage system," *J. Mod. Power Syst. Clean Energy*, vol. 4, pp. 529–541, 2016.

[9] E. (GDF S. Puchala, "Stockage d'Electricité par Air comprimé avec Récupération de la CHaleur de compression," 2009.

[10] A. Ter-Gazarian, *Energy storage power systems*. 1994.

[11] F. Crotogino, "Le stockage d'air comprimé de HUNTOR: plus de 20 ans de succès dans l'exploitation," p. 4, 2001.

[12] INERIS (Institut national de l'environnement industriel et des Risques), "Stockage souterrain de l'air comprimé dans le contexte de la transition énergétique," 2016.

[13] S. Crane, D. Fong, and E. Berlin, "Energy storage system utilizing compressed gas," no. US 8,247,915 B2. p. 31, 2012.

[14] S. Lemofouet, "Investigation and optimisation of hybrid electricity storage systems based on compressed air and supercapacitors," École polytechnique fédérale de Lausanne, Lausanne, 2006.

[15] SustainX, "Energy storage and generation systems and methods using coupled cylinder

assemblies," 2013.

[16] J. Guanwei, X. Weiqing, C. Maolin, and S. Yan, "Micron-sized water spray-cooled quasi-isothermal compression for compressed air energy storage," *Exp. Therm. Fluid Sci.*, vol. 96, pp. 470–481, 2018.

[17] X. Zhang *et al.*, "A near-isothermal expander for isothermal compressed air energy storage system," *Appl. Energy*, vol. 225, pp. 955–964, 2018.

[18] C. Qin and E. Loth, "Liquid piston compression efficiency with droplet heat transfer," *Appl. Energy*, vol. 114, pp. 539–550, 2014.

[19] Emmanuel Barraud, "L'Etat de Vaud soutient le stockage d'énergie par air comprimé," 2014. [Online]. Available: https://actu.epfl.ch/news/l-etat-de-vaud-soutient-le-stockage-d-energie-par-/. [Accessed: 03-Mar-2020].

[20] S. Lemofouet and A. Rufer, "Projet pilote de stockage hydropneumatique d'énergie pour le lissage de la production photovoltaïque de Mont-Soleil," 2011.

[21] S. Lemofouet, "Réalisation et Caractérisation Etendue d'un Prototype de Système de Stockage Hydro-pneumatique d'Energie," Switzerland, 2012.

[22] S. Lemofouet and A. Rufer, "Multistage hydraulic gas compression/expansion system and methods," US 8,567,183,B2, 2013.

[23] B. Cretinon, "Paramètres hygrométriques," vol. 33, no. R3047 V1, p. 12, 2004.

[24] A. Odukomaiya, A. Abu-Heiba, S. Graham, and A. M. Momen, "Experimental and analytical evaluation of a hydro-pneumatic compressed-air Ground-Level Integrated Diverse Energy Storage (GLIDES) system," *Appl. Energy*, vol. 221, pp. 75–85, 2018.

[25] J. de Ven and P. Li, "Liquid Piston Gas Compression," *Appl. Energy*, vol. 86, pp. 2183–2191, 2009.

[26] G. Dib, "Thermodynamic simulation of compressed air energy storage systems," INSA Lyon, 2020.